

# Supernova neutrinos and the turbulence power spectrum: point source statistics

James P. Kneller\* and Neel V. Kabadī†

*Department of Physics, North Carolina State University, Raleigh, North Carolina 27695, USA*

(Dated: December 7, 2024)

The neutrinos emitted from the proto-neutron star created in a core-collapse supernova must run through a significant amount of turbulence before exiting the star. Turbulence can modify the flavor evolution of the neutrinos imprinting itself upon the signal we will detect here at Earth. The turbulence effect upon individual neutrinos, and the correlation between pairs of neutrinos, is sensitive to the power spectrum of the turbulence and recent analysis of the turbulence in a two-dimensional hydrodynamical simulation of a core-collapse supernova indicates the power spectrum may not be the Kolmogorov 5/3 inverse power law as has been previously assumed. We study the effect of non-Kolmogorov turbulence power spectra upon individual neutrinos from a point source and find reasonable values for the turbulence amplitudes indicate supernova neutrinos and antineutrinos do possess sensitivity to the power spectrum when the turbulence is in the vicinity of the Mikheyev, Smirnov and Wolfenstein (MSW) resonances.

PACS numbers: 47.27.-i,14.60.Pq,97.60.Bw

## I. INTRODUCTION

There is now ample evidence from both observations and simulations for the multi-dimensional nature of core-collapse supernovae. For example, high-velocity “jets” of sulfur-rich material - which presumably originated deep in the stellar mantle - are seen in the supernova remnant Cassiopeia A [1], the double-peaked structure of the Oxygen and Magnesium nebular lines in observations of SN 2003jd could be understood if the star exploded aspherically [2], and spectropolarimetric observations of stripped-envelope core-collapse supernovae also indicate aspherical explosions [3]. Asphericity in the hydrodynamical simulations of core collapse supernovae is seen to emerge even when the progenitor is spherically symmetric [4–14]. An aspherical explosion of a star will naturally lead to the generation of turbulence which, in turn, alters the flavor evolution of neutrinos racing through the stellar mantle from the cooling proto-neutron star formed at the core.

Finding the consequence of the turbulence upon the neutrinos is vital for interpreting the signal from the next supernova in the Galaxy. This need has long been recognized and various authors have examined the effect of turbulence upon the neutrinos [15–23]. From these studies it has emerged that turbulence can affect the neutrinos in two different ways. The first, more direct effect of the turbulence is to ‘stimulate’ transitions between the instantaneous neutrino eigenstates [22, 23] while the neutrino is propagating through the turbulent region. Although this effect depends upon a number of factors, typically noticeable turbulence effects require the density fluctuations must be present in the region of the supernovae mantle where neutrinos experience the Mikheyev,

Smirnov and Wolfenstein (MSW) resonances [30, 31] and their amplitude must be of order a few percent. That said, the description of the stimulated transition effect of turbulence is not in terms of MSW resonances and MSW resonances are not required for the effect to appear.

The second, more subtle effect of turbulence occurs when the neutrino transition probabilities exhibit phase effects [24, 25]. In order to observe phase effects and this second, indirect, sensitivity to turbulence we require at least two semi-adiabatic MSW resonances and/or density discontinuities in the profile. Even then, it is sometimes possible to reduce the imprint of this second effect by carefully selecting the profile and neutrino energy. In more general circumstances we find both effects simultaneously though the second effect of turbulence becomes most obvious when the amplitude is small because the direct effect is usually negligible in this limit [19].

While the basic effects of turbulence upon the neutrinos have been determined, it is not apparent to what extent they might operate in a supernova due to the lack of suitable multi-dimensional, high resolution, long duration hydrodynamical simulations. In their absence authors have been forced to model the turbulence in a supernova by adopting a turbulence-free profile and then inserting turbulence into it in the form of a random field with assumed properties. The problem with this approach is that the validity of these prescriptions for the turbulence in supernovae are unknown. That situation changed recently with the study by Borriello *et al.* [26] of the turbulence in a two-dimensional simulation from Kifonidis *et al.* [27] which possessed the necessary resolution and duration. Borriello *et al.* fitted the power spectrum for the turbulence along each radial slice with a broken inverse-power law defined by four parameters. Two of these parameters correspond to spectral indices which they called  $p_1$  and  $p_2$ :  $p_1$  is the index for the longer wavelengths and the other,  $p_2$ , for the shorter. The other two parameters are the amplitude and the break wavenumber defined in terms of a multiple of the long wavelength

---

\*Electronic address: jpknelle@ncsu.edu

†Electronic address: nvkabadi@ncsu.edu

cutoff scale. The short wavelength index was found to have a mean and  $1 - \sigma$  error of around  $p_2 = 3.04^{+0.57}_{-0.63}$  while the index for the longer wavelengths was found to have a mean and  $1 - \sigma$  error of  $p_1 = 1.85^{+0.54}_{-0.77}$ .

The analysis by Boriello *et al.* is a welcome addition to the literature but the well-known differences between the properties of turbulence in two and three spatial dimensions means it is not clear which results can be safely carried over to 3D. For example, in the inertial range of wavenumbers for 2D turbulence one may observe a Kraichnan inverse enstrophy cascade which funnels turbulent power into the long wavelength modes, a Kolmogorov energy cascade in the opposite direction, and even double cascades [28] where turbulence is injected at some given scale and cascades to both longer *and* shorter wavelengths. The turbulence seen by Boriello *et al.* appears to be of this double cascade type because they find broken power laws similar to a Nastrom-Gage spectrum [29]. If the presence of the ‘break wavenumber’ and a short wavelength index  $p_2$  is due to the 2D nature of the turbulence and if the amplitude they obtain is similarly contaminated by 2D effects, this leaves, perhaps, just the long wavelength index  $p_1$  as being reliable. Thus, the most conservative conclusion to draw from the study is that the long wavelength spectral index has a mean of  $p_1 \sim 5/3$  and the fact that it has a range appears to indicate the turbulence is also not always ‘fully developed’. The results of Boriello *et al.* indicate it is reasonable to explore something other than a Kolmogorov,  $5/3$ , power spectrum in the prescriptions for turbulence in 3D which has heretofore been the default. Changing the power spectrum will alter the evolution of individual neutrinos passing through the turbulence and the correlation between pairs of neutrinos sent along parallel rays.

The analytic results of Friedland & Gruzinov [17] and Patton, Kneller & McLaughlin [23] can be used to predict the effect of changing the spectral index for the direct effect of turbulence. They indicate that a hardening of the power spectrum should increase the turbulence effect upon the neutrinos by i) increasing the amplitude of the turbulence modes which lead to transitions between the neutrino states, ii) permitting more combinations of modes to drive transitions without a severe simultaneous narrowing of the resonance, and iii) lowering the amplitude of the modes which suppress those transitions. However the precise amount by which the direct turbulence effect alters the neutrino transition properties as the power spectrum changes has not been determined, and nothing exists for the indirect turbulence effect. It is the filling of this hole which is the goal of this paper focused upon neutrinos from a point source. We begin by describing the calculations we have performed paying particular attention to the turbulence power spectrum we use and other details. The following section demonstrates the two effects of turbulence and describes two models which we shall use to understand our results and make predictions. Our results for the change in the ensembles for single neutrinos at three different energies

and a wide range of turbulence amplitudes as a function of the power spectral index are then presented and we finish with a summary and our conclusions.

## II. DESCRIPTION OF THE CALCULATIONS

In order to study the effect of the supernova turbulence upon the neutrinos we compute the transition probabilities which are the set of probabilities that a neutrino initially in some state  $\nu_j$  is later detected in some other state  $\nu_i$  at a different location. These quantities are denoted as  $P_{ij}$  for neutrinos and  $\bar{P}_{ij}$  for the antineutrinos. The transition probabilities can be computed from the elements of the  $S$  matrix which links the initial and final neutrino states, that is  $P_{ij} = |S_{ij}|^2$ , and the  $S$  matrix is computed by solving the Schrodinger equation

$$i \frac{dS}{d\lambda} = HS \quad (1)$$

where  $H$  is the Hamiltonian and  $\lambda$  the affine parameter along the neutrino trajectory. In our case the Hamiltonian possesses two contributions: the first,  $H_0$ , is from the vacuum and the second,  $H_{MSW}$  comes from the effect of the matter upon the neutrino [30, 31]. We do not include the contribution to  $H$  from ‘collective’ effects: see Duan, Fuller & Qian [32] for a review of this fascinating subject. The vacuum Hamiltonian for a neutrino of a given energy  $E$  is defined by the two independent mass squared differences  $\delta m_{ij}^2 = m_i^2 - m_j^2$  of  $\delta m_{32}^2$  and  $\delta m_{21}^2$ . It is diagonal in the ‘mass’ basis which is related to the flavor basis by the Maki-Nakagawa-Sakata-Pontecorvo [33, 34] unitary ‘mixing’ matrix  $U$ . The mixing matrix can be written in terms of three vacuum mixing angles,  $\theta_{12}$ ,  $\theta_{13}$  and  $\theta_{23}$ , a CP phase  $\delta$ , and two Majorana phases though the two Majorana phases do not influence the evolution [35, 37]. Throughout this paper we adopt numerical values of  $\delta m_{21}^2 = 7.5 \times 10^{-5} \text{ eV}^2$ ,  $\delta m_{32}^2 = 2.32 \times 10^{-3} \text{ eV}^2$  (a normal hierarchy),  $\theta_{12} = 33.9^\circ$ ,  $\theta_{13} = 9^\circ$  and  $\theta_{23} = 45^\circ$  which are consistent with the Particle Data Group [34]. The CP phase is set to zero. The MSW potential  $H_{MSW}$  is diagonal in the flavor basis because matter interacts with neutrinos based on their flavor. The matter affects the neutrinos via both neutral and charged current channels but the neutral current contribution to  $H_{MSW}$  may be ignored because it leads to an unobservable global phase. In contrast, the absence of mu and tau leptons in the matter means the charged current potential affects the electron flavor neutrino and antineutrinos only. The charged current potential for the electron flavor neutrinos and antineutrinos is given by  $V_{ee} \pm \sqrt{2}G_F n_e(r)$  where  $G_F$  is the Fermi constant and  $n_e(r)$  the electron density. The plus sign applies to the electron neutrinos, the minus sign for the electron antineutrinos. The tiny radiative  $\mu\tau$  potential [38, 39] is ignored since it is a factor of  $\sim 10^{-5}$  smaller than the potential affecting the electron flavor in the standard model

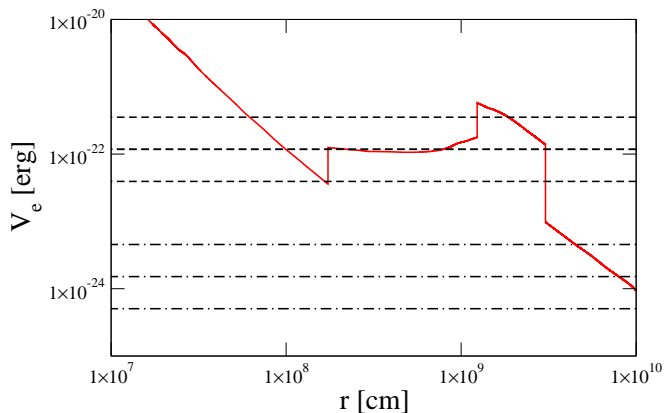


FIG. 1: The MSW potential for the snapshot at  $t = 3$  s post-bounce of the  $M = 10.8 M_{\odot}$  simulation from Fischer *et al.* [44] as a function of distance. From the inside out, the three discontinuities in the profile are the reverse shock at  $r_r = 1,734$  km, the contact discontinuity at  $r_c = 12,348$  km, and the forward shock at  $r_f = 30,323$  km. From top to bottom, the horizontal dashed lines are the two-flavor resonance potential for a neutrino with  $E = 5$  MeV,  $E = 15$  MeV, and  $E = 45$  MeV respectively using mixing parameters  $\delta m^2 = 2.32 \times 10^{-3}$  eV<sup>2</sup> and  $\theta = 9^{\circ}$  while the the horizontal dot-dashed lines are the two-flavor resonance potential for a neutrino with  $E = 5$  MeV,  $E = 15$  MeV, and  $E = 45$  MeV from top to bottom respectively using mixing parameters  $\delta m^2 = 7.5 \times 10^{-5}$  eV<sup>2</sup> and  $\theta = 33.9^{\circ}$ .

(but may be two or three orders of magnitude bigger if supersymmetric contributions are included [40]).

It is through the electron density  $n_e(r)$  that the turbulence enters  $H_{MSW}$ . As noted in the Introduction, the ideal would be to use density profiles taken from high resolution, long duration, multi-dimensional simulations of supernovae in order to study the effect of turbulence. Alternatively one could adopt a profile from a one-dimensional simulation and add turbulence to it and this method is the one we shall adopt. We shall introduce the turbulence in such a way that the profile from the 1D simulation is also the mean electron density  $\langle n_e(r) \rangle$ , the average here being over realizations of the turbulence. The profile we use for  $\langle n_e(r) \rangle$  is the  $t = 3$  s postbounce snapshot from the  $10.8 M_{\odot}$  simulation by Fischer *et al.* [44]. This profile is shown in figure (1) and was chosen so that neutrinos with energies 5 MeV, 15 MeV and 45 MeV would be affected by the turbulence we inserted to various degrees. The reader will observe there are three discontinuities within it: the reverse shock at  $r_r = 1,734$  km, the contact discontinuity at  $r_c = 12,348$  km and the forward shock at  $r_f = 30,323$  km. These features were steepened by hand from the original simulation data: see Lund & Kneller [22] for a discussion of why this steepening was necessary. It is in the region between the forward and reverse shocks that strong turbulence is seen [26, 45, 46]. As in Lund & Kneller [22], we use two random field realizations: one for the zone between the forward shock and the contact

discontinuity, and a second between the contact discontinuity and the reverse shock. Realizations are generated by multiplying  $\langle n_e(r) \rangle$  by a factor  $1 + F(r)$  where  $F(r)$  is a Gaussian random field with a power spectrum  $E$ . Quite generally we may write the random field  $F(r)$  within the region  $r_{<}$  to  $r_{>}$  as a Fourier series of the form

$$F(r) = C_{\star} \tanh\left(\frac{r - r_{<}}{\lambda_{\star}}\right) \tanh\left(\frac{r_{>} - r}{\lambda_{\star}}\right) \times \sum_{a=1}^{N_q} \sqrt{V_a} \{A_a \cos(q_a r) + B_a \sin(q_a r)\}. \quad (2)$$

The purpose of the two tanh functions is to damp the fluctuations close to discontinuities at  $r_{<}$  and  $r_{>}$  and the parameter  $\lambda_{\star}$  is the damping scale which we set to  $\lambda_{\star} = 100$  km. The parameter  $C_{\star}$  is the root-mean-square amplitude of the field and we shall use the same value of  $C_{\star}$  for the two realizations for simplicity. The set of co-efficients  $\{A\}$  and  $\{B\}$  are independent standard, zero-mean Gaussian random variates (which ensures the mean value of  $F$  is zero), the wavenumbers for the Fourier modes are  $q_a$  and the quantities  $V_a$  are ‘volume’ co-efficients. The method for generating a realization of the turbulence is the same ‘variant C’ of the Randomization Method described in Kramer, Kurbanmuradov, & Sabelfeld [41] and used in Kneller & Mauney [42]. The space of wavenumbers is divided into  $N_q$  regions and from each region we select a random wavenumber  $q$  using the normalized power-spectrum,  $E(q)$ , as a probability distribution. The volume parameters  $V_a$  are the integrals of the power spectrum over each region. In order to produce random fields that affect the neutrinos we must cover a sufficiently large dynamic range of scales. Given the size of the turbulence regions shown in figure (1) and the neutrino oscillation lengthscale of  $\sim 10$  km at these densities, the dynamic range is found to be of order 40-50 decibels which requires at a minimum that  $N_q$  also be in the range 40-50 [43]. The power spectrum of the random field is taken to be an inverse power law of the form

$$E(q) = \frac{(\alpha - 1)}{2 q_{\star}} \left(\frac{q_{\star}}{|q|}\right)^{\alpha} \Theta(|q| - q_{\star}). \quad (3)$$

Here  $\alpha$  is the spectral index and  $q_{\star}$  is the long wavelength, small wavenumber, cutoff. The parameter  $q_{\star}$  is sometimes called the ‘driving scale’ since it is the longest, non-zero turbulence wavelength. In our case this wavelength is twice the size of the turbulence domains, that is,  $1/q_{\star} = 2(r_{>} - r_{<})$ .

With the Hamiltonian including turbulence constructed our plan is to generate multiple realizations of the turbulence and then solve equation (1) for the  $S$ -matrix for each realization. This approach will allow us to construct ensembles of results which we can then characterize with frequency distributions or with distribution moments. The transition probabilities we report are for the ‘matter’ basis states. The matter basis states are

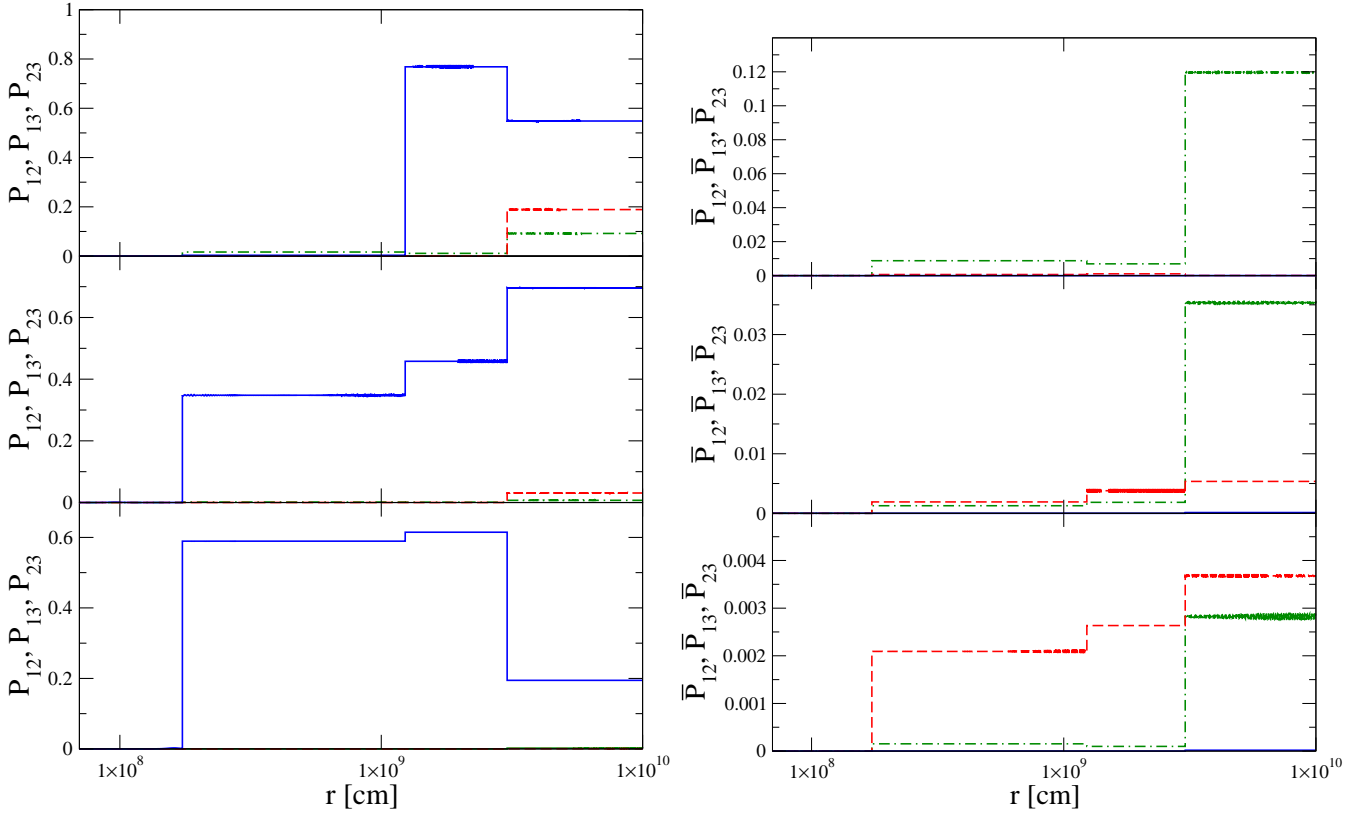


FIG. 2: In the left figure we show the evolution of the neutrino transition probability  $P_{12}$  (dashed dot),  $P_{13}$  (dashed) and  $P_{23}$  (solid) with energies of 5 MeV (top panels) 15 MeV (middle panels) and 45 MeV (bottom panels) through the profile shown in figure (1). The right figure we show the evolution of the antineutrino transition probabilities  $\bar{P}_{12}$  (dashed dot),  $\bar{P}_{13}$  (dashed) and  $\bar{P}_{23}$  (solid) with energies of 5 MeV (top panels) 15 MeV (middle panels) and 45 MeV (bottom panels) through the same profile.)

related to the flavor basis states by the matter mixing matrix  $\tilde{U}$  which is defined so that the flavor basis Hamiltonian  $H^{(f)}$  and its eigenvalue matrix  $\tilde{K}$  are related via  $H^{(f)} = \tilde{U}\tilde{K}\tilde{U}^\dagger$  [36, 37]. The evolution of neutrinos and antineutrinos with energies 5 MeV, 15 MeV and 45 MeV and the given set of mixing parameters through the base profile are shown in figure (2). For the neutrinos the mixing between  $\nu_2$  and  $\nu_3$  dominates and note that the sudden discontinuities in the transition probability  $P_{23}$  occur at the discontinuities in the profile and not at the MSW resonances (unless the two coincide). For 5 MeV neutrinos there is a noticeable change in both  $P_{12}$  and  $P_{13}$  at the forward shock; for the 15 MeV the change in the same probabilities at the same location is much smaller and by 45 MeV the change in  $P_{12}$  and  $P_{13}$  are minuscule. In the antineutrinos we again see a noticeable jump in  $\bar{P}_{12}$  at the forward shock of similar size to the change of  $P_{12}$  for neutrinos of the same energy while the jump in  $\bar{P}_{12}$  at higher energies is much smaller; any jump in  $\bar{P}_{23}$  is very small at all antineutrino energies (the mixing in this channel is suppressed if the mixing in  $\nu_2 - \nu_3$  is strong); and similarly the jumps in  $\bar{P}_{13}$  are small for all energies. For future reference, the values of the transition probabilities  $\{P_{12}, P_{13}, P_{23}\}$  and  $\{\bar{P}_{12}, \bar{P}_{13}, \bar{P}_{23}\}$  through

this profile for 5 MeV neutrinos are  $\{0.0918, 0.189, 0.548\}$  and  $\{0.120, 7.09 \times 10^{-5}, 3.12 \times 10^{-5}\}$  respectively, for 15 MeV neutrinos they are  $\{7.13 \times 10^{-3}, 0.0308, 0.696\}$  and  $\{0.0353, 5.36 \times 10^{-3}, 1.35 \times 10^{-4}\}$ , for 45 MeV neutrinos they are  $\{2.22 \times 10^{-3}, 6.73 \times 10^{-4}, 0.194\}$  and  $\{2.81 \times 10^{-3}, 3.68 \times 10^{-3}, 1.85 \times 10^{-5}\}$ . For the antineutrinos all transition probabilities are ?.

The evolution of the neutrinos and antineutrinos through the underlying base profile will determine the extent to which turbulence is able to modify the emerging probabilities. In general we find that if  $P_{ij}$  is close to the limits of zero or unity then the effect of turbulence tends to be smaller, everything else being equal. Thus we should expect big effects in  $P_{23}$  even at small turbulence amplitudes while effects in  $P_{12}$ ,  $P_{13}$  and the antineutrinos will require somewhat larger density fluctuations.

### III. THE TWO EFFECTS OF TURBULENCE

Before presenting the results from numerical calculations, we first take time to demonstrate the two effects of turbulence. As we previously stated, the first effect is the modification of the neutrino transition probability evolu-

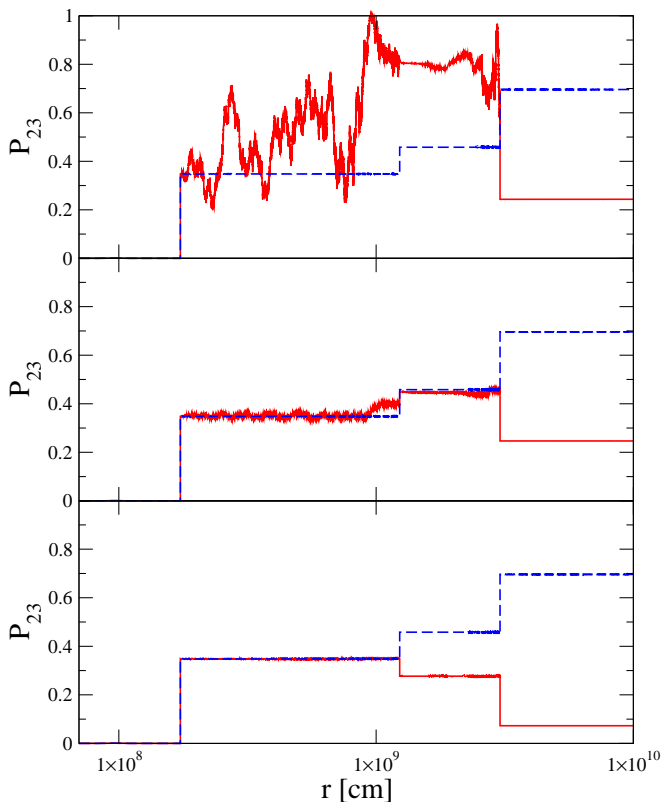


FIG. 3: The evolution of  $P_{23}$  as a function of distance  $r$  for a 15 MeV neutrino. The dashed line is the evolution through the underlying profile and the solid line is the evolution with a single realization of turbulence with spectral index  $\alpha = 5/3$ . In the top panel  $C_* = 10\%$ , in the middle  $C_* = 1\%$  and in the bottom  $C_* = 0.1\%$

tion in the region of the turbulence due to direct stimulation between the states, and the second is the modification of the transition probabilities of the neutrino as it emerges from a turbulent region if the transition probabilities are subject to phase effects. The two effects are neatly shown in figure (3) where we see the evolution of the transition probability  $P_{23}$  as a function of distance through the profile shown in figure (1) for a  $E = 15$  MeV neutrino. In the top panel where  $C_* = 0.1$  we see the first case: the evolution of the transition probability with turbulence differs from the evolution without turbulence as soon as the neutrino enters the turbulence region. In the middle panel where  $C_* = 10^{-2}$  we see a small differences between the evolution with and without turbulence as soon as the neutrino enters the turbulence but the jumps at the discontinuities are much bigger. In the bottom panel where  $C_* = 10^{-3}$  there is no apparent difference between the evolution with and without turbulence *until* the contact discontinuity. Beyond that point the two curves are different but exhibit no relative change until the neutrino passes through the forward shock. In these bottom two panels the change in the evolution is mainly due to a change in the phase effects; phase effects do occur in the top panel but are subdominant. But note well

that that even though the turbulence amplitude differs by two orders of magnitude between the three calculations, the value of  $P_{23}$  that emerges is very similar in each case. Let us now construct two useful models that can be used to understand how turbulence affects the neutrinos as seen in figure (3).

### A. Phase effect distortion

Let us first concentrate on the distortion of the phase effect and we shall use a two-flavor model for simplicity. In this case the neutrino passes through a set of discontinuities at the entrance and exit of the turbulent regions but is not modified by the turbulence between them. We can construct an  $S$ -matrix which describes this evolution and then derive the transition probability. First, the matter basis  $S$  matrix describing the evolution across a discontinuity located at  $r$  is  $S(r_+, r_-) = \tilde{U}^\dagger(r_+) \tilde{U}^\dagger(r_-)$  where  $\tilde{U}$  is the matter mixing matrix,  $r_-$  is a point immediately before the discontinuity and  $r_+$  a point immediately after. Adiabatic evolution of the neutrino between discontinuities means the  $S$ -matrix must be of the form

$$S(r_b, r_a) = \begin{pmatrix} \exp(-i\phi_1) & 0 \\ 0 & \exp(-i\phi_2) \end{pmatrix} \quad (4)$$

where

$$\phi_j = \int_{r_a}^{r_b} \tilde{k}_j(r) dr \quad (5)$$

and  $\tilde{k}_j(r)$  is the instantaneous eigenvalue for matter state  $j$ . Thus the  $S$ -matrix describing the neutrino evolution through a profile with two discontinuities, located at  $r_a$  and  $r_b$  is

$$S \sim \tilde{U}^\dagger(r_{b+}) \tilde{U}^\dagger(r_{b-}) \begin{pmatrix} \exp(-i\phi_1) & 0 \\ 0 & \exp(-i\phi_2) \end{pmatrix} \times \tilde{U}^\dagger(r_{a+}) \tilde{U}^\dagger(r_{a-}) \quad (6)$$

where we have omitted the evolution up to  $r_{a-}$  and beyond  $r_{b+}$  assuming it to be adiabatic. If we denote by  $P_a$  and  $P_b$  the crossing probabilities through the discontinuities separately, we find the crossing probability for the entire profile is

$$P = P_a (1 - P_b) + (1 - P_a) P_b + 2\sqrt{P_a P_b (1 - P_a)(1 - P_b)} \cos(\Phi). \quad (7)$$

where  $\Phi = \phi_1 - \phi_2 + \text{constant}$ . We take the phase  $\Phi$  to be a random variate distributed according to a von Mises distribution

$$f(\Phi) = \frac{\exp(\kappa \cos(\Phi - \Phi_0))}{2\pi I_0(\kappa)} \quad (8)$$

where  $\Phi_0$  is the mean value of  $\Phi$  and  $\kappa$  is the concentration. Defining  $P_* = P_a (1 - P_b) + (1 - P_a) P_b$  and  $\Delta =$

$2\sqrt{P_a P_b (1 - P_a)(1 - P_b)}$  and noting  $|dP/d\Phi| = \Delta \sin \Phi$ , we find the distribution for  $P$  is

$$f(P) = \frac{1}{2\pi I_0(\kappa) \sqrt{\Delta^2 - (P - P_\star)^2}} \times \exp\left(\kappa \cos\left[\cos^{-1}\left(\frac{P - P_\star}{\Delta}\right) - \Phi_0\right]\right) \quad (9)$$

on the interval  $P_\star - \Delta \leq P \leq P_\star + \Delta$ . In the limit where  $\kappa \rightarrow 0$ , the distribution of  $\Phi$  is rectangular and the probability distribution for  $P$  becomes the arcsine distribution i.e.

$$f(P) = \frac{1}{2\pi \sqrt{\Delta^2 - (P - P_\star)^2}} \quad (10)$$

which has a mean of  $P_\star$  and variance of  $V(P) = \Delta^2/2$ .

In the other limit where the concentration is large we can expand the phase  $\Phi$  around  $\Phi_0$  so that to lowest order (assuming  $\sin \Phi_0 \neq 0$ )

$$P - P_0 = -\Delta \sin(\Phi_0) (\Phi - \Phi_0) \quad (11)$$

where  $P_0 = P_\star + \Delta \cos \Phi_0$ . This equation shows  $P$  and  $\Phi$  are linearly related in this limit and so the standard deviation of  $P$  is proportional to the standard deviation of  $\Phi$ :  $\sigma_P \propto \sigma_\Phi$ . The phase difference  $\Phi$  between two discontinuities is given by

$$\Phi \propto \int_{r_a}^{r_b} (\tilde{k}_i(r) - \tilde{k}_j(r)) dr \quad (12)$$

and for neutrinos far from a MSW resonance - such as the 45 MeV neutrinos in the  $\nu_2 - \nu_3$  mixing channel - the difference between  $\tilde{k}_2$  and  $\tilde{k}_3$  is approximately the MSW potential  $\langle V \rangle (1 + F)$  in the region where we place the turbulence. This means we can write an expression for the variance of  $\Phi$  which is

$$\langle (\Phi - \Phi_0)^2 \rangle \approx \left\langle \left( \int_{r_a}^{r_b} \langle V \rangle (r) F(r) dr \right)^2 \right\rangle \quad (13)$$

The integral is dominated by the longer wavelengths, lowest wavenumbers of the random field  $F$  - the integral over the turbulence modes with wavelengths smaller than the scale height of the potential will be very small. If we ignore all the Fourier modes except the lowest then we predict  $\langle (\Phi - \Phi_0)^2 \rangle \propto \langle A_1^2 \rangle$  and, since  $q_1 \approx q_\star$ , we have  $\langle A_1^2 \rangle \propto \alpha - 1$ . Putting this together with the linear relationship between  $P$  and  $\Phi$  we conclude

$$\sigma_P \propto \sqrt{\alpha - 1}. \quad (14)$$

This result seems to indicate harder spectra have less effect upon the transition probability than softer spectra. This makes sense because when the turbulence effect is dominated by phase distortion the neutrinos are more sensitive to the longest wavelengths of the turbulence whose amplitude *increases* with  $\alpha$ .

Obviously the distorted phase effect of turbulence requires a phase effect be present in the transition probability in the absence of turbulence. Glancing at figure (2) we see only  $P_{23}$  has a strong phase effect with two or more semi-adiabatic transitions at the three energies we are using, plus  $P_{12}$  and  $\bar{P}_{12}$  for the 5 MeV neutrinos: in all other mixing channels the jumps in  $P_{ij}$  at the discontinuities are too small. Thus we expect to see the distorted phase effect of turbulence for all three energies we are using in the  $\nu_2 - \nu_3$  mixing channel, and maybe a small distorted phase effect in  $\nu_1 - \nu_2$  mixing at 5 MeV.

## B. Direct stimulation

A detailed description of direct stimulation of transitions between neutrino states can be found in Kneller, McLaughlin & Patton [21] and Patton, Kneller & McLaughlin [23]. The effect can be understood as similar to that of the effect of a laser upon a polarized molecule and is very powerful because it is able to describe the effect of turbulence on a case-by-case basis: for every pair of neutrino matter states  $i$  and  $j$  there is an associated splitting  $\delta k_{ij}$  between two eigenvalues of the Hamiltonian. As equation (2) indicates, the turbulence can be described as a Fourier series and transitions between the neutrino states will be seen if a set of integers  $\{n\}$  can be found, one for each Fourier mode, such that  $\delta k_{ij} + \sum_a n_a q_a \approx 0$ . When the condition is exact, known as a parametric resonance [47–51], the amplitude of the transition between states  $i$  and  $j$  is 100% no matter the amplitudes of each Fourier mode. Where the amplitudes of the modes enter is through the distance  $\lambda$  over which a neutrino makes the transition from state  $i$  to state  $j$ . This distance is inversely proportional to the coupling between the two states i.e.  $U_{ei} U_{ej}^\star$  where  $U_{ei}$  are elements of the ‘matter mixing matrix’ and also inversely proportional to a product of Bessel functions  $J_{n_a}(z_a)$  where  $z_a \propto C_a/q_a$  and the integer  $n_a$  is the same integer previously identified. Incidentally, the inverse proportionality of the transition wavelength to  $U_{ei} U_{ej}^\star$  indicates that stimulated transitions occur over shorter distances when the underlying density is close to the MSW density because the product takes on its maximal value at that location. Finally, the only difference when one considers antineutrinos is that the splitting  $\delta k_{ij}$  and coupling  $U_{ei} U_{ej}^\star$  are computed using a Hamiltonian where the MSW potential switches sign.

The power spectral index  $\alpha$  appears via the amplitudes of the Fourier modes  $C_a$  whose expectation values are  $\langle C_a \rangle^2 = C_\star^2 (q_\star/q_a)^\alpha$ . At small  $C_\star$  one typically finds the integers  $n_a = 0$  for all  $a$  *except* for the mode whose wavenumber is closest to the eigenvalue splitting  $\delta k_{ij}$ . The smallness of  $C_a$  indicates  $z_a$  for that mode will be small so using  $J_1 \sim z$  for small  $z$  we find the transition wavelength  $\lambda$  is inversely proportional to that mode’s amplitude  $C_a$  which depends upon  $\alpha$ . Decreasing  $\alpha$  puts more power into the modes corresponding to the

neutrino eigenvalue splitting so we should expect to see an increase the size of the stimulated transition effect. Increasing  $C_\star$  should cause the same effect. but it should be noted that the presence of large amplitude, long wavelength turbulence modes can *suppress* transitions even when the parametric resonance condition is fulfilled [23] which can complicate the relationship between  $C_\star$  and the size of the stimulated transition effect. The evolution of the underlying profile introduces a further complication: the splitting between the neutrino eigenvalues  $\delta k_{ij}$  and the coupling  $U_{ei} U_{ej}^\star$  between the matter states both evolve with  $\langle V \rangle$  and at present it is only possible to predict where and with what approximate strength the transitions occur, not the actual change in the transition probability. Phenomenologically one finds the distributions of the transition probabilities are exponential when the transition probability in the absence of turbulence is either zero or unity [19].

The stimulated transitions work between the discontinuities in the profile while the evolution across the discontinuities is still  $\tilde{U}^\dagger(r_+) \tilde{U}^\dagger(r_-)$ . In effect one replaces the central  $S$ -matrix in equation (6) which describes adiabatic evolution between the discontinuities with a matrix that may or may not have non-zero off diagonal elements depending upon whether there were any stimulated transitions in the turbulence region. If there were no transitions the effect of the turbulence is solely to distort the phase if applicable; if there were transitions then we get something different.

In the limit of strong turbulence transitions occur so often - the parametric resonance condition is fulfilled many times through the profile - and in virtually all realizations of the turbulence. In this limit one finds the  $S$ -matrix for the evolution between the discontinuities becomes essentially random rendering the evolution across the discontinuities unimportant. In this strong turbulence limit an ensemble of  $S$ -matrices approaches that of an ensemble of  $N$ -flavor circular unitary matrices [52] where the distribution of every element of the matrices is identical. This limiting behavior of the  $S$ -matrices can be used to derive the distributions of the transition probabilities in the strong turbulence limit. First, we note that the  $N$  real components,  $x_{ij}$ , plus the  $N$  imaginary components,  $y_{ij}$ , of the elements of a row or column in every  $S$ -matrix form a  $2N$  Euclidean space. The requirement of unitarity of the  $S$ -matrix is equivalent to the definition that a vector made from these real and imaginary components lies upon the surface of a unit sphere in this space. Since these  $2N$  quantities are identically distributed, the probability  $f$  of a particular set of the elements from a row or column must be uniform over the surface of the sphere. For example, if we chose to look at a column  $j$  then the probability that we are located at  $\{x_{1j}, y_{1j}, x_{2j}, y_{2j}, \dots\}$ , must be proportional to the area element  $dA$  allowing us

to write

$$f(x_{1j}, y_{1j}, x_{2j}, y_{2j}, \dots) d^N x d^N y \propto dA \\ = \delta \left( 1 - \sum_{i=1}^N x_{ij}^2 - \sum_{i=1}^N y_{ij}^2 \right) \prod_{i=1}^N dx_{ij} \prod_{i=1}^N dy_{ij}. \quad (15)$$

If we now change variables so that each of the  $N$  independent pairs  $x_{ij}, y_{ij}$  are expressed as

$$x_{1j} = \sqrt{P_{1j}} \cos \theta_{1j}, \quad y_{1j} = \sqrt{P_{1j}} \sin \theta_{1j}, \quad (16)$$

$$x_{2j} = \sqrt{P_{2j}} \cos \theta_{2j}, \quad y_{2j} = \sqrt{P_{2j}} \sin \theta_{2j}, \quad (17)$$

then the  $P_{ij}$ 's are found to be distributed as

$$f(P_{1j}, \dots, P_{Nj}) d^N P \propto \delta \left( 1 - \sum_{i=1}^N P_{ij} \right) \prod_{i=1}^N dP_{ij}. \quad (18)$$

The set of transition probabilities  $\{P_{1j}, \dots, P_{Nj}\}$  are uniformly distributed on the surface of a standard  $N - 1$  simplex. Equation (18) can be integrated over  $N - 1$  of the  $P$ 's and normalized so that we derive the final result that element  $P_{ij}$  must be distributed according to

$$f(P_{ij}) = (N - 1) (1 - P_{ij})^{N-2}. \quad (19)$$

The shape of the distribution is controlled by the number of flavors  $N$  that are involved and nothing else. With the distribution for  $P_{ij}$  found it is a simple task to determine that the mean and variance are

$$\langle P_{ij} \rangle = \frac{1}{N}, \quad (20)$$

$$V(P_{ij}) = \sigma_{ij}^2 = \frac{N - 1}{N^2 (N + 1)} \quad (21)$$

For the specific case of  $N = 2$  the distribution is uniform with mean  $1/2$  and variance  $1/12$ ; for  $N = 3$  the distribution is triangular with mean  $1/3$  and variance  $1/18$ .

Since there are three flavors of neutrino it would seem we should use the  $N = 3$  case but in practice whether 3-flavor depolarization is actually reached depends upon the placement of the turbulence in the profile in relation to the H and L resonance densities for a given energy. If not located in the appropriate place in the profile for a given neutrino energy, two flavor depolarization may be more appropriate. As we stated, the distance over which a neutrino makes the transition from matter state  $j$  to matter state  $i$  is proportional to the product of instantaneous mixing matrix elements  $U_{ei} U_{ej}^\star$ . This product has its maximal value at the resonance between states  $i$  and  $j$ . Figure (1) shows that the H resonance density for the  $E = 45$  MeV neutrinos is below the densities where we place the turbulence by a factor  $\gtrsim 3$ , the L resonance density is lower by a factor  $\gtrsim 300$ . For  $E = 45$  MeV neutrinos we should expect some difficulty stimulating transitions between matter states  $\nu_1$  and  $\nu_2$  but somewhat easier for mixing between states  $\nu_2$  and  $\nu_3$ . For the lower energy of 15 MeV the H resonance density is

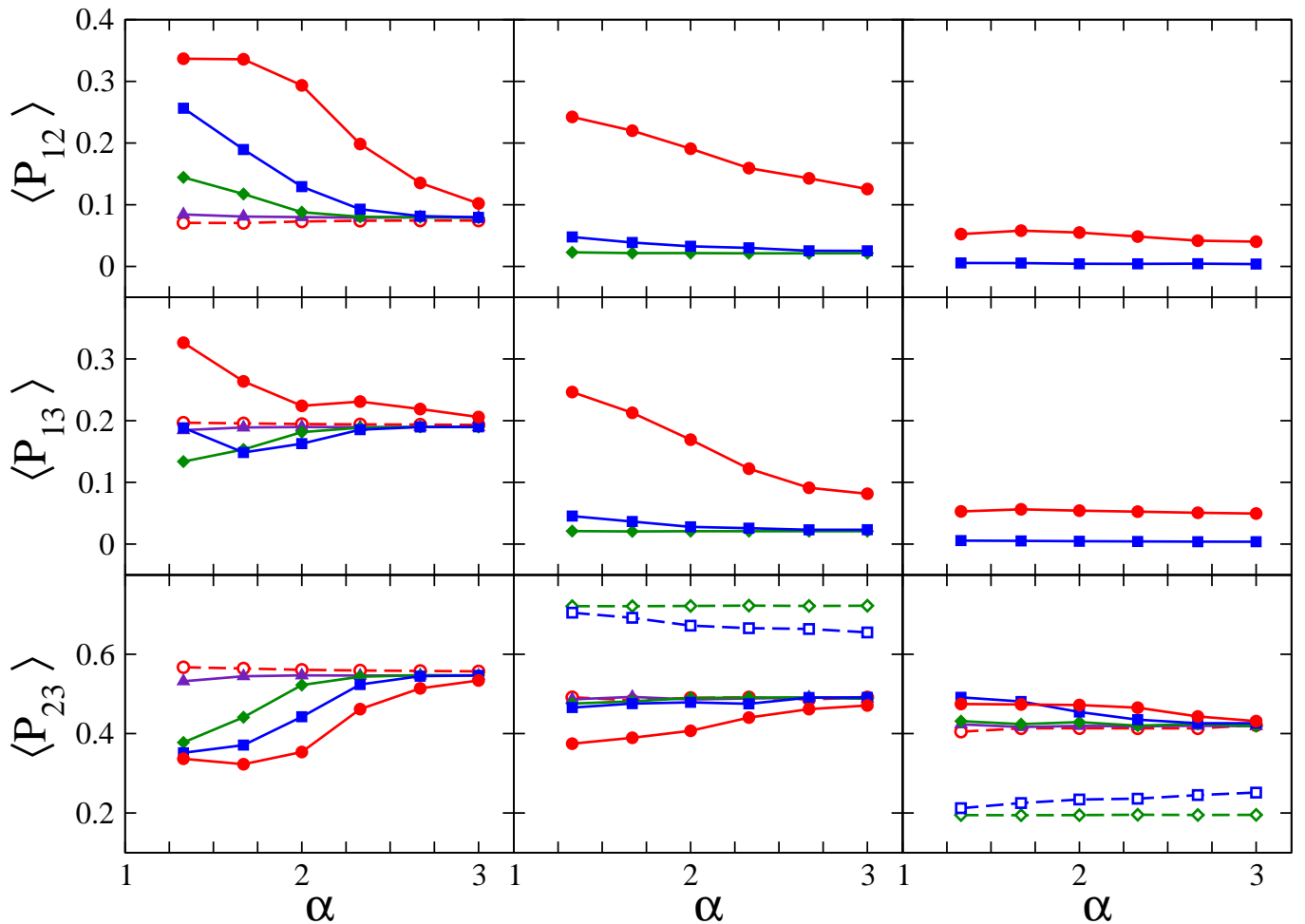


FIG. 4: The mean values of  $P_{12}$  (top row),  $P_{13}$  (middle row) and  $P_{23}$  (bottom row) as a function of the power spectral index. The leftmost column is for 5 MeV neutrinos, the middle for 15 MeV and the rightmost is 45 MeV. In all panels the curves correspond to  $C_\star = 0.5$  (filled circles),  $C_\star = 0.3$  (filled squares),  $C_\star = 0.1$  (filled diamonds),  $C_\star = 10^{-2}$  (filled triangles),  $C_\star = 10^{-3}$  (open circles),  $C_\star = 10^{-4}$  (open squares) and  $C_\star = 10^{-5}$  (open diamonds). For the sake of clarity, not all lines appear in each panel; where a line is missing it should be taken to be negligibly different from the smallest value of  $C_\star$  shown in the panel.

very similar to the density of the profile between the reverse shock and the contact discontinuity which would lead us to expect a strong stimulated transition effect in this channel for this energy. The L resonance for this same energy again lies below the density of the profile meaning the product of mixing matrix elements  $U_{e1}U_{e2}^*$  will be small again suppressing stimulated transitions between  $\nu_1$  and  $\nu_2$ . Finally, the H resonance density for the 5 MeV neutrinos is similar to the density of the profile *and* the difference between the L resonance density and the profile density between the reverse shock and the contact discontinuity is only of order a factor of a few. Thus of the three energies we are considering, the 5 MeV neutrinos have the best prospect of exhibiting stimulated transitions between all three states and reaching 3 flavor depolarization, the 15 MeV and  $E = 45$  MeV neutrinos should show evidence for stimulated transition between two states.

Finally, we sometimes find circumstances where the distributions for the transition probabilities in a given channel exhibit mixing between two more fundamental distributions: see for example figure (12) in Kneller & Volpe [19]. These situations arise because strong turbulence effects, especially stimulated transitions, are often ‘all-or-nothing’. Mixing between distributions will shift the means and variances of the total distribution from expected values. If the distribution Type A, with mean transition probability  $\langle P \rangle_A$  and variance  $\sigma_A^2$ , contributes a fraction  $f$  to the total distribution, and a different distribution, Type B, with mean transition probability  $\langle P \rangle_B$  and variance  $\sigma_B^2$  contributes  $1 - f$ , then the mean transition probability of the total distribution is  $\langle P \rangle = f \langle P \rangle_A + (1 - f) \langle P \rangle_B$  and similarly the variance is also  $\sigma^2 = f \sigma_A^2 + (1 - f) \sigma_B^2$ . One should expect the fraction  $f$  to depend upon the neutrino energy and snapshot time as well as the turbulence amplitude  $C_\star$  and the spectral index  $\alpha$ .

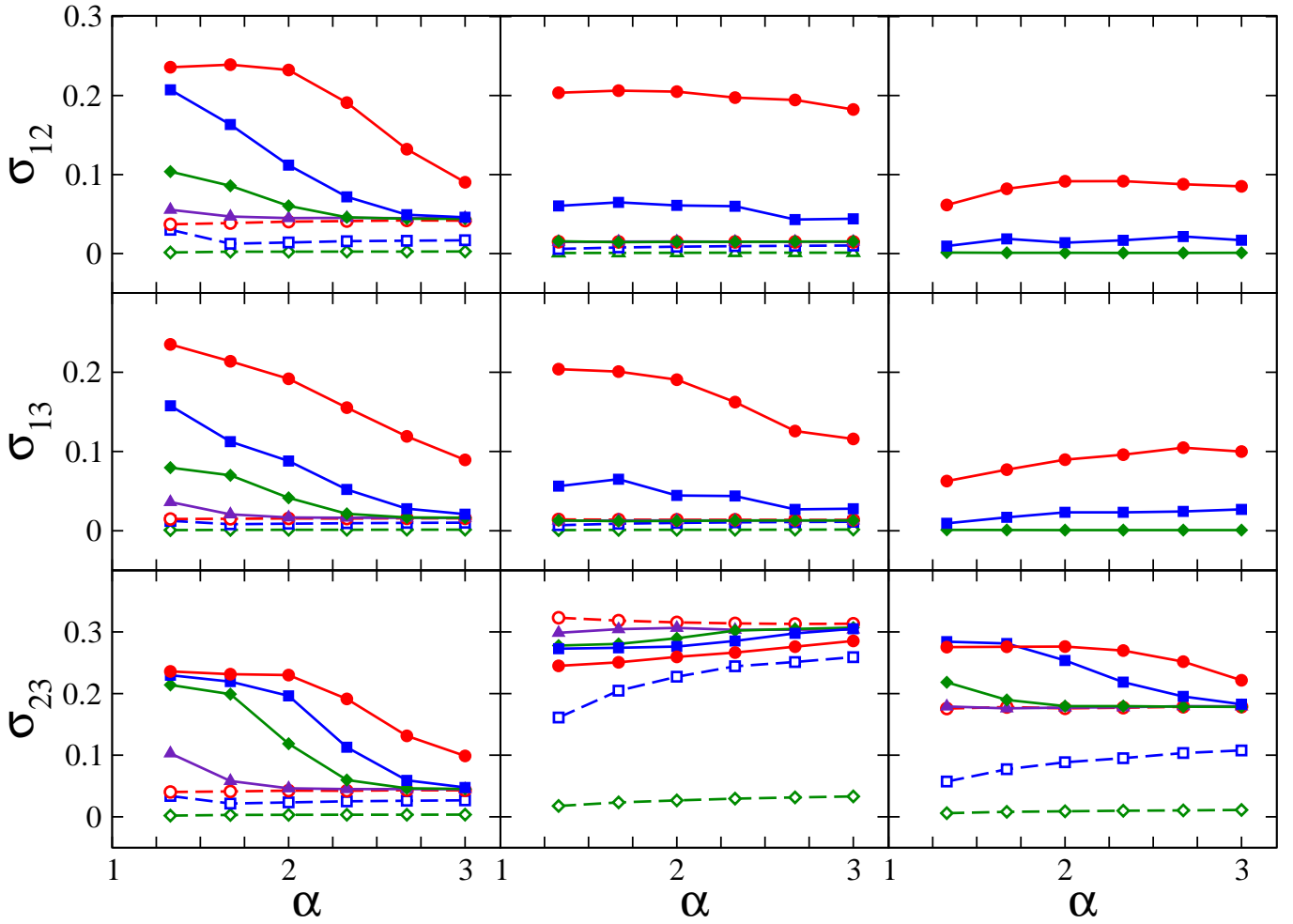


FIG. 5: The standard deviation of  $P_{12}$  (top row),  $P_{13}$  (middle row) and  $P_{23}$  (bottom row) as a function of the power spectral index. The leftmost column is for 5 MeV neutrinos, the middle for 15 MeV and the rightmost is 45 MeV. In all panels the curves correspond to  $C_\star = 0.5$  (filled circles),  $C_\star = 0.3$  (filled squares),  $C_\star = 0.1$  (filled diamonds),  $C_\star = 10^{-2}$  (filled triangles),  $C_\star = 10^{-3}$  (open circles),  $C_\star = 10^{-4}$  (open squares) and  $C_\star = 10^{-5}$  (open diamonds). Again, for the sake of clarity, not all lines appear in each panel; where a line is missing it should be taken to be negligibly different from the smallest value of  $C_\star$  shown in the panel.

## IV. RESULTS

### 1. $E = 45$ MeV

#### A. Neutrinos

In figures (4) and (5) we show the mean values and standard deviation of the distributions of the neutrino transition probabilities  $P_{12}$ ,  $P_{13}$  and  $P_{23}$  as a function of the spectral index and the turbulence amplitude for the three representative energies we are using. Even a cursory glance indicates there is a great deal of rich behavior as a function of the three parameters we have varied to generate the figures and we shall show there is evidence in both figures of the two different effects of turbulence poking through.

Let us first examine  $P_{23}$  for  $E = 45$  MeV. At large amplitudes and hard spectral indices, the figures show the  $\nu_2$ - $\nu_3$  mixing channel reaches the two-flavor depolarized limit where  $\langle P_{23} \rangle = 0.5$  and  $\sigma_{23} = 0.28$  when  $C_\star = 50\%$  and  $\alpha \leq 7/3$  and  $C_\star = 30\%$  and  $\alpha \leq 5/3$ . At these same large amplitudes we do see some evolution of  $\langle P_{23} \rangle$  and  $\sigma_{23}$  with  $\alpha$  that is in line with what we expect from the stimulated transition model i.e. at larger  $\alpha$  the mean and standard deviation are both slightly smaller than the 2-flavor depolarized values indicating a slightly reduced effect of turbulence because of the reduced amplitude of the modes that have wavelengths of order the eigenvalue splittings. But when we look in the range  $0.1\% \lesssim C_\star \lesssim 10\%$  it appears  $P_{23}$  is independent of  $\alpha$  fixed at the apparently arbitrary  $\langle P_{23} \rangle = 0.44$  with a standard deviation  $\sigma_{23}$  which is also independent of  $\alpha$

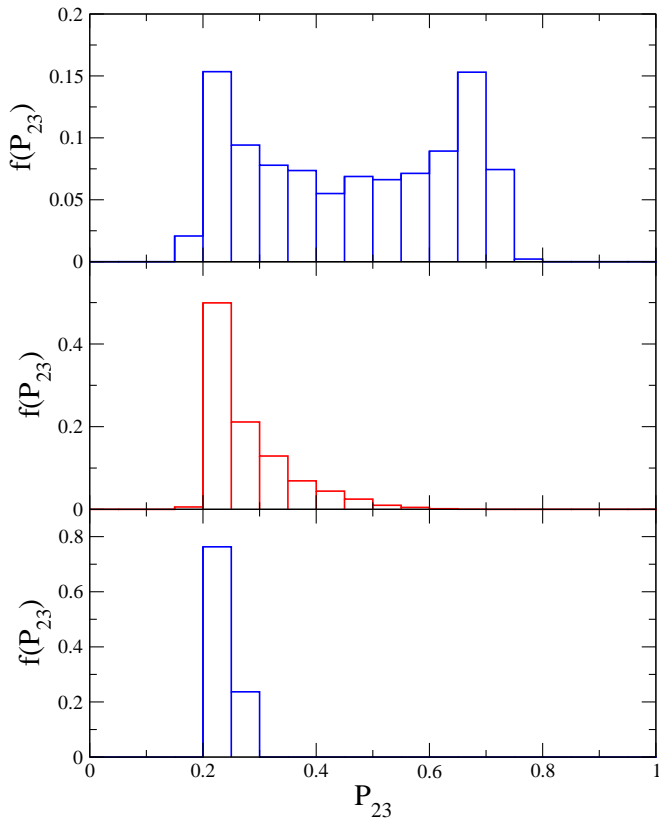


FIG. 6: Frequency distribution of the transition probability  $P_{23}$  for the case of a 45 MeV neutrino. The spectral index is set to  $\alpha = 5/3$  and, from top to bottom, the turbulence amplitude is  $C_\star = 10^{-3}$ ,  $C_\star = 10^{-4}$  and  $C_\star = 10^{-5}$ .

fixed at a similarly arbitrary value of  $\sigma_{23} \approx 0.18$ . Only at very small turbulence amplitudes,  $C_\star \lesssim 0.01\%$  do we see the dependence upon  $C_\star$  and  $\alpha$  re-emerge. In fact at  $C_\star = 0.01\%$  it appears both  $\langle P_{23} \rangle$  and the standard deviation  $\sigma_{23}$  increase as the power spectrum becomes softer which is contrary to the evolution at higher amplitudes. This behavior of  $\langle P_{23} \rangle$  and  $\sigma_{23}$  for  $C_\star \leq 10\%$  is not what we would expect from the stimulated transition model so must be explained by using the distorted phase model.

From analyzing the profile without turbulence we find the  $E = 45$  MeV neutrinos change substantially at the reverse and forward shocks as shown in figure (2). The transition probabilities at these two locations are  $P_a = 0.57$  and at the second  $P_b = 0.93$ . Using the distorted phase model we can combine these results to give  $P_\star = 0.44$  and  $\Delta = 0.25$ . Since the transition probability in the absence of turbulence is  $P_{23} = 0.20$  we deduce  $\Phi = 163^\circ$ . With this information in hand we predict the distribution of the transition probability  $P_{23}$  when we insert the turbulence will lie in the range of  $P_\star - \Delta = 0.19$  to  $P_\star + \Delta = 0.69$ . When the concentration  $\kappa$  is small we expect an arcsine distribution for  $P_{23}$  with a mean  $\langle P_{23} \rangle = P_\star = 0.44$  and standard deviation  $\Delta/\sqrt{2} = 0.18$ . These predictions match the data well and imply that in the range  $0.1\% \lesssim C_\star \lesssim 10\%$  the 45 MeV neutrinos are

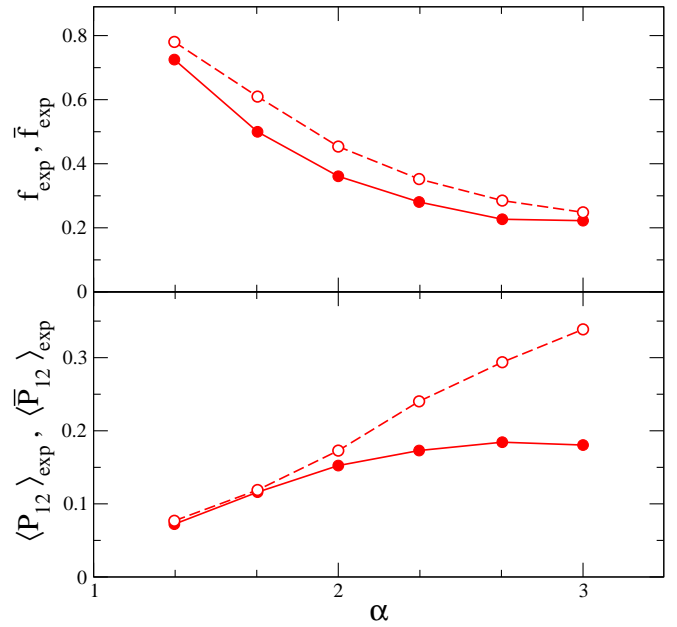


FIG. 7: Top panel, the fraction of  $E = 45$  MeV neutrinos (filled circles) and antineutrinos (open circles) with transition probabilities  $P_{12}$  or  $\bar{P}_{12}$  distributed according to an exponential as a function of the spectral index when and  $C_\star = 0.5$ . Bottom panel, the mean value of the exponentially distributed  $E = 45$  MeV neutrinos (filled circles) and antineutrinos (open circles) when  $C_\star = 0.5$ .

experiencing a strong distorted phase effect. At smaller turbulence amplitudes when the concentration  $\kappa$  is larger the distribution will be like a half-Gaussian because the turbulence-free value of  $P_{23} = 0.20$  is close to the lower limit of the distribution. The frequency distribution of  $P_{23}$  for 45 MeV neutrinos at  $C_\star = 10^{-3}$ ,  $C_\star = 10^{-4}$  and  $C_\star = 10^{-5}$  is shown in figure (6) and this expected shape of the distributions is seen in the numerical results. At these same smaller turbulence amplitudes the running of  $\langle P_{23} \rangle$  and  $\sigma_{23}$  with  $\alpha$  for the  $E = 45$  MeV neutrinos is also in line with the prediction from the distorted phase model because the prediction that  $\sigma_{23} \propto \sqrt{\alpha - 1}$  appears to be correct at small  $C_\star$ , e.g.  $C_\star = 10^{-4}$ .

Compared to  $P_{23}$ , the mean of the transition probabilities  $\langle P_{12} \rangle$  and  $\langle P_{13} \rangle$  for the  $E = 45$  MeV neutrinos appear quite unremarkable differing from the turbulence free limit only when  $C_\star = 0.5$  and then possessing only a soft dependence upon  $\alpha$ . The standard deviations  $\sigma_{12}$  and  $\sigma_{13}$  evolve similarly. At this energy the distorted phase effect of turbulence does not operate in these channels because the jumps in  $P_{12}$  and  $P_{13}$  across the discontinuities are small. The sensitivity to the turbulence is entirely through the stimulated transition mechanism. But not every neutrino is effected because the distributions for these two transition probabilities are found to be mixtures of very narrow distribution which peaks at zero and an exponential distribution. We fit for the fraction of neutrinos with transition probabilities

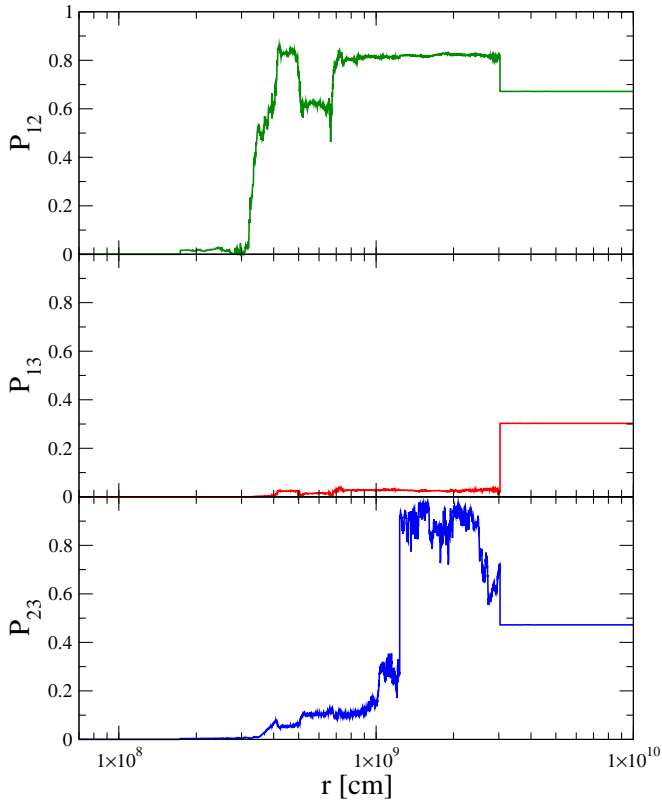


FIG. 8: The evolution of  $P_{12}$  (top panel),  $P_{13}$  (middle panel), and  $P_{23}$  (bottom panel) as a function of distance  $r$  through a single realization of turbulence with spectral index  $\alpha = 5/3$  and  $C_\star = 0.3$ . The neutrino energy is 5 MeV.

distributed according to the exponential,  $f_{exp}$ , and find for  $E = 45$  MeV and  $C_\star = 0.5$  that  $f_{exp} = 22\%$  at  $\alpha = 3$  and  $f_{exp} = 73\%$  at  $\alpha = 4/3$  the fraction  $f_{exp}$  varies as  $f_{exp} \propto 1/\alpha^{3/2}$ . As the spectral index increases the fraction of neutrinos affected by the turbulence decreases but at the same time, the mean value of  $P_{12}$  of the exponentially distributed subset *increases* with  $\alpha$ :  $\langle P_{12} \rangle_{exp} = 7\%$  at  $\alpha = 4/3$  which has changed to  $\langle P_{12} \rangle_{exp} = 18\%$  at  $\alpha = 3$ . These two trends are shown in figure (7). The simultaneous decrease of  $f_{exp}$  and increase of  $\langle P_{12} \rangle_{exp}$  as the power spectrum softens almost cancel and leads to the overall soft dependence of  $\langle P_{12} \rangle$  and  $\sigma_{12}^2$  with  $\alpha$  seen in figures (4) and (5).

## 2. $E = 5$ MeV

We switch now to the 5 MeV neutrinos. Here neither the H resonance nor the L resonance are too far from the densities where we insert the turbulence so the product of instantaneous mixing matrix elements  $U_{ei}U_{ej}^\star$  are not small in any mixing channel. Thus we expect circumstances might be reached where stimulated transitions in all three channels could occur and that we may reach three-flavor depolarization at large amplitudes. When

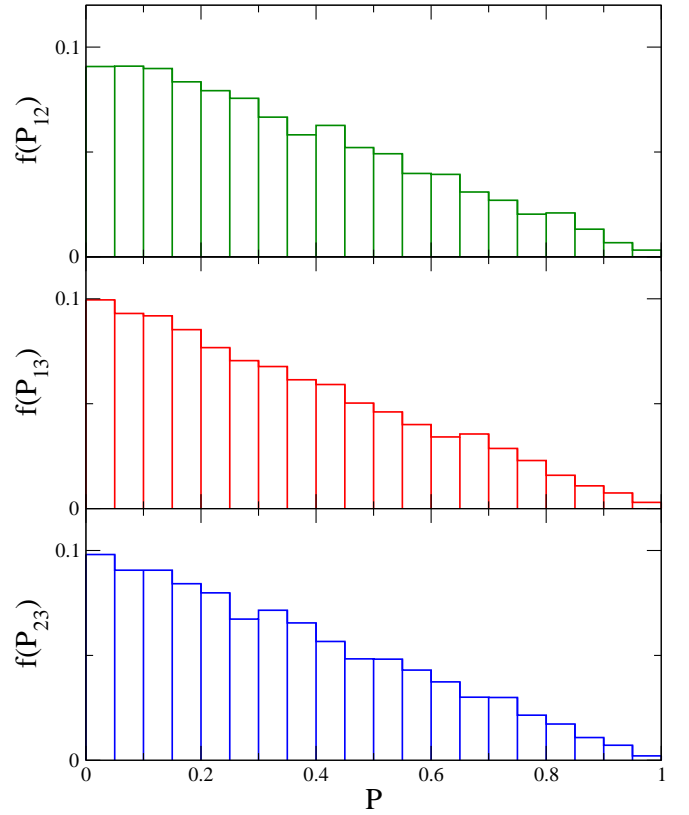


FIG. 9: The frequency distribution of the transition probabilities  $P_{12}$ ,  $P_{13}$  and  $P_{23}$  for the case of a 5 MeV neutrino. The spectral index is  $\alpha = 4/3$  and the turbulence amplitude is  $C_\star = 0.5$ .

we look we indeed find examples such as figure(8) where stimulated transitions occur in multiple channels at the same time. One notices both  $P_{12}$  and  $P_{23}$  tend to evolve in sudden jumps which correspond to the locations of the parametric resonances and that the jump in  $P_{12}$  occurs *before* the jump in  $P_{23}$ . This ordering occurs because the neutrinos pass through the rarefied region between the reverse shock and contact discontinuity before they pass through the pile up between the contact discontinuity and forward shock.

This strong mixing for individual neutrinos indicates the explanation for the saturation of the mean values of  $P_{12}$ ,  $P_{13}$  and  $P_{23}$  at  $\langle P_{ij} \rangle = 1/3$  when  $C_\star = 50\%$  and  $\alpha \leq 5/3$  seen in figure (4), and the standard deviations at  $\sigma_{ij} = 0.23$  in figure (5) in the same range of amplitudes and spectral indices is the transition to three flavor depolarization. We confirm this conclusion by showing the actual frequency distribution of the transition probabilities for the particular case of  $C_\star \gtrsim 50\%$  and  $\alpha = 4/3$  and observe all three transition probabilities are triangular as predicted. Figures (4) and (5) reveal the three-flavor depolarized limit is reached for  $P_{12}$  only for  $C_\star = 50\%$  and  $\alpha \leq 5/3$  whereas the same limit appears somewhat easier to reach for  $P_{23}$  because even  $C_\star = 10\%$  amplitude turbulence saturates at  $\langle P_{23} \rangle = 1/3$  and  $\sigma_{23} = 0.23$  for

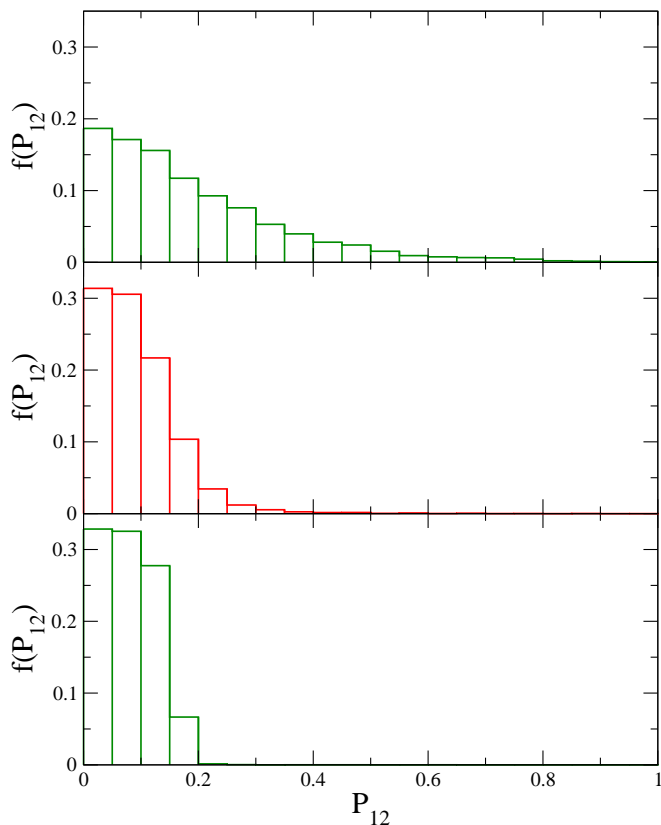


FIG. 10: The frequency distribution of  $P_{12}$  for  $E = 5$  MeV neutrinos at  $C_\star = 0.3$ . In the top panel  $\alpha = 5/3$ , in the middle  $\alpha = 7/3$ , and in the bottom panel  $\alpha = 3$ .

$\alpha = 4/3$  or at  $C_\star = 50\%$  we are able to relax the spectral index to  $\alpha = 2$ . This is not surprising given the location of the turbulence in the profile with respect to the  $\nu_2 - \nu_3$  mixing resonance density shown in figure (1). Note also the figures indicate the evolution to three flavor depolarization did not pass through a two flavor intermediate stage because we do not see  $\langle P_{23} \rangle \approx 0.5$  or  $\sigma_{23} \approx 0.28$  as one would expect.

At sufficiently small amplitudes for the turbulence,  $C_\star \lesssim 1\%$ , we see all three transition probabilities of the 5 MeV neutrinos approach the previously reported values through the underlying profile. The convergence is more rapid for softer power spectra: e.g. at  $C_\star = 10\%$  the mean of  $P_{12}$  and  $P_{23}$  are measurably different from the turbulence free values at  $\alpha = 5/3$  but not so at  $\alpha = 7/3$ . However it would be a mistake to conclude that turbulence effects have disappeared just because the mean transition probability in the ensembles is the same as the transition probability without turbulence. A glance at the standard deviations in figure (5) reveals that it is not until  $C_\star \lesssim 0.001\%$  that the turbulence effect actually disappears for this energy because both  $\sigma_{23} \neq 0$  and  $\sigma_{12} \neq 0$  until this limit. Between  $0.001\% \lesssim C_\star \lesssim 1\%$  the distributions of the transition probabilities are simply *centered* on the turbulence-free limits. Again, this acute sensitivity to small  $C_\star$  is due to the distorted phase effect with the twist

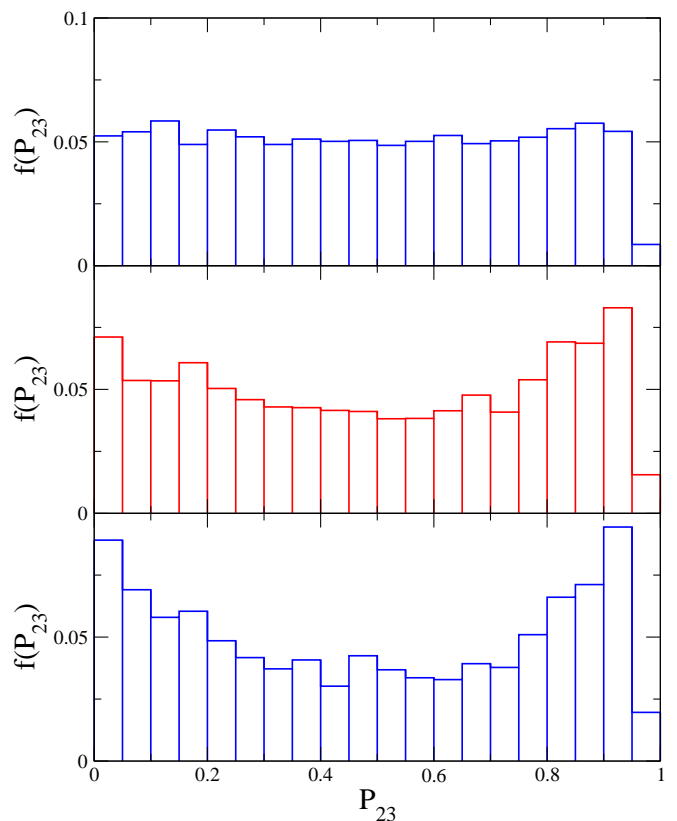


FIG. 11: The frequency distribution of  $P_{23}$  for 15 MeV neutrinos at  $\alpha = 5/3$ . In the top panel  $C_\star = 10\%$ , in the middle panel  $C_\star = 1\%$ , and in the bottom panel  $C_\star = 0.1\%$ ,

that now both  $P_{23}$  and  $P_{12}$  (and  $\bar{P}_{12}$ ) are affected. The distributions of  $P_{12}$  and  $P_{23}$  when  $0.001\% \lesssim C_\star \lesssim 10\%$  are mixtures of an exponential and the distorted phase distributions and the evolution of  $\langle P_{12} \rangle$  and  $\langle P_{23} \rangle$  are actually due to the evolution of the exponentially distributed subset, not the subset where the turbulence only distorts the phase. This can be seen in figure (10) where we show the distributions for  $P_{12}$  for the  $E = 5$  MeV neutrinos at three values of  $\alpha$  when  $C_\star = 0.3$ . In contrast to the  $E = 45$  MeV neutrinos, there is no simple formula relating the ensemble mean and standard deviation to the mean and standard deviation of the exponentially distributed subset.

### 3. $E = 15$ MeV

Finally, the energy  $E = 15$  MeV is somewhat different than the other two. For this energy the mean value of  $P_{23}$  is approximately  $\langle P_{23} \rangle = 0.5$  at  $\alpha = 3$  even for turbulence amplitudes as small as  $C_\star = 0.1\%$ . Only at  $C_\star = 0.5$  and small  $\alpha$  does  $P_{23}$  drop toward the three-flavor depolarization limit of  $\langle P_{23} \rangle = 1/3$ ,  $\sigma_{23} = 0.23$  while  $\langle P_{12} \rangle$  and  $\langle P_{13} \rangle$  also creep in this direction. Returning to focus upon  $P_{23}$  we see this energy is much more sensitive to turbulence than the other other two energies

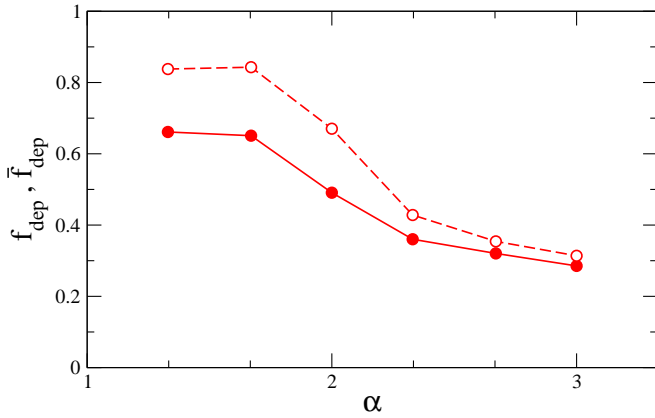


FIG. 12: The fraction of neutrinos (filled circles) and antineutrinos (open circles) with energy  $E = 15$  MeV which have a transition probability  $P_{12}$  or  $\bar{P}_{12}$  that is distributed according to a depolarized distribution. The turbulence amplitude is set to  $C_\star = 0.5$ .

because even turbulence amplitudes of  $C_\star = 0.01\%$  shift  $\langle P_{23} \rangle$  from the turbulence-free limit. Like the 45 MeV neutrinos, there is a range of turbulence amplitudes, in this case  $30\% \gtrsim C_\star \gtrsim 0.1\%$  where  $\langle P_{23} \rangle$  is independent of  $C_\star$ . However looks can be deceptive and if we look at the evolution of the standard deviations of the ensembles in figure (5) we see something very strange. At  $C_\star = 30\%$  the standard deviation is  $\sigma_{23} = 0.28$  at  $\alpha = 4/3$ , the value expected for a uniform distribution, but, at fixed  $\alpha$ , as  $C_\star$  decreases the standard deviation increases! Only when  $C_\star \lesssim 0.1\%$  does the standard deviation drop and at very small turbulence amplitudes the  $\sigma_{23} \propto \sqrt{\alpha - 1}$  trend re-emerges.

This evolution of the distributions of  $P_{23}$  is explained by a transition from stimulated transitions at large  $C_\star$ /small  $\alpha$  to the distorted phase effect at smaller  $C_\star$ /larger  $\alpha$  and can be seen in figure (11). The mean value of  $P_{23}$  is approximately the same in all three cases, around  $\langle P_{23} \rangle \approx 0.5$ , but the distributions are clearly different depending upon  $C_\star$ : for the large amplitude  $C_\star = 0.1$  the distribution is almost uniform - the bin  $0.95 \leq P_{23} \leq 1$  appears low - whereas the distribution for  $C_\star = 0.001$  has a very peculiar shape with the extreme values of  $P_{23}$  more common than the mean. The distribution in the top panel is due to the direct effect of turbulence, the distribution in the lower is the indirect effect via the change in the phase effects and is consistent with an arcsine distribution, similar to that seen in the top panel of figure (6), albeit on the interval of zero to unity.

That the mean and standard deviation for  $P_{12}$  do not match those of our model distributions is again due to the mixing of distributions. At  $C_\star = 0.5$  inspection indicates the mixing distributions in this channel for this energy are a sharp distribution which peaks at zero and a three flavor depolarized distribution. The fraction of  $E = 15$  MeV neutrinos at  $C_\star = 0.5$  with  $P_{12}$  distributed according to the depolarized distribution,  $f_{dep}$ , is shown

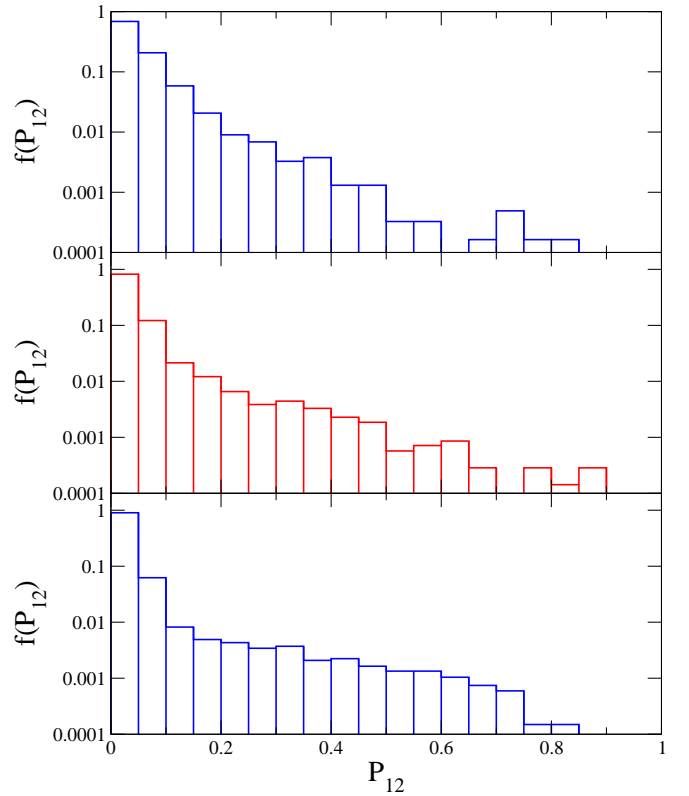


FIG. 13: The frequency distribution of the neutrino transition probability  $P_{12}$  when  $E = 15$  MeV and  $C_\star = 0.3$ . In the top panel  $\alpha = 4/3$ , in the middle  $\alpha = 5/3$ , and in the bottom panel  $\alpha = 2$ .

in figure (12). As for the  $E = 45$  MeV neutrinos, the smaller the spectral index the more likely the mixing in the  $\nu_1 - \nu_2$  channel will be affected by the turbulence: the difference is that the mixing distributions do not also evolve with  $\alpha$  at this value of  $C_\star$ . When we consider the smaller value of  $C_\star = 0.3$  we find the mixing distributions for  $P_{12}$  are now a narrow distribution peaked at zero and an exponential. The frequency distributions of  $P_{12}$  at  $C_\star = 0.3$  and  $E = 15$  MeV at three values of  $\alpha$  are shown in figure (13) where we observe a flattening of the exponentially distributed component as  $\alpha$  increases similar to that seen in the lower panel of figure (7) for  $E = 45$  MeV when  $C_\star = 0.5$ . The fraction of  $E = 15$  MeV neutrinos which have an exponentially distributed  $P_{12}$  varies from  $f_{exp} = 12\%$  at  $\alpha = 4/3$  to  $f_{exp} = 2\%$  at  $\alpha = 3$  which, again, indicates that softer power spectra disrupted fewer neutrinos by the stimulated transition effect. These fractions are much greater than those in the same channel at  $E = 45$  MeV for the same  $C_\star$ .

## B. Anti-neutrinos

Even though we are considering just a normal hierarchy, large amplitude turbulence certainly does affect

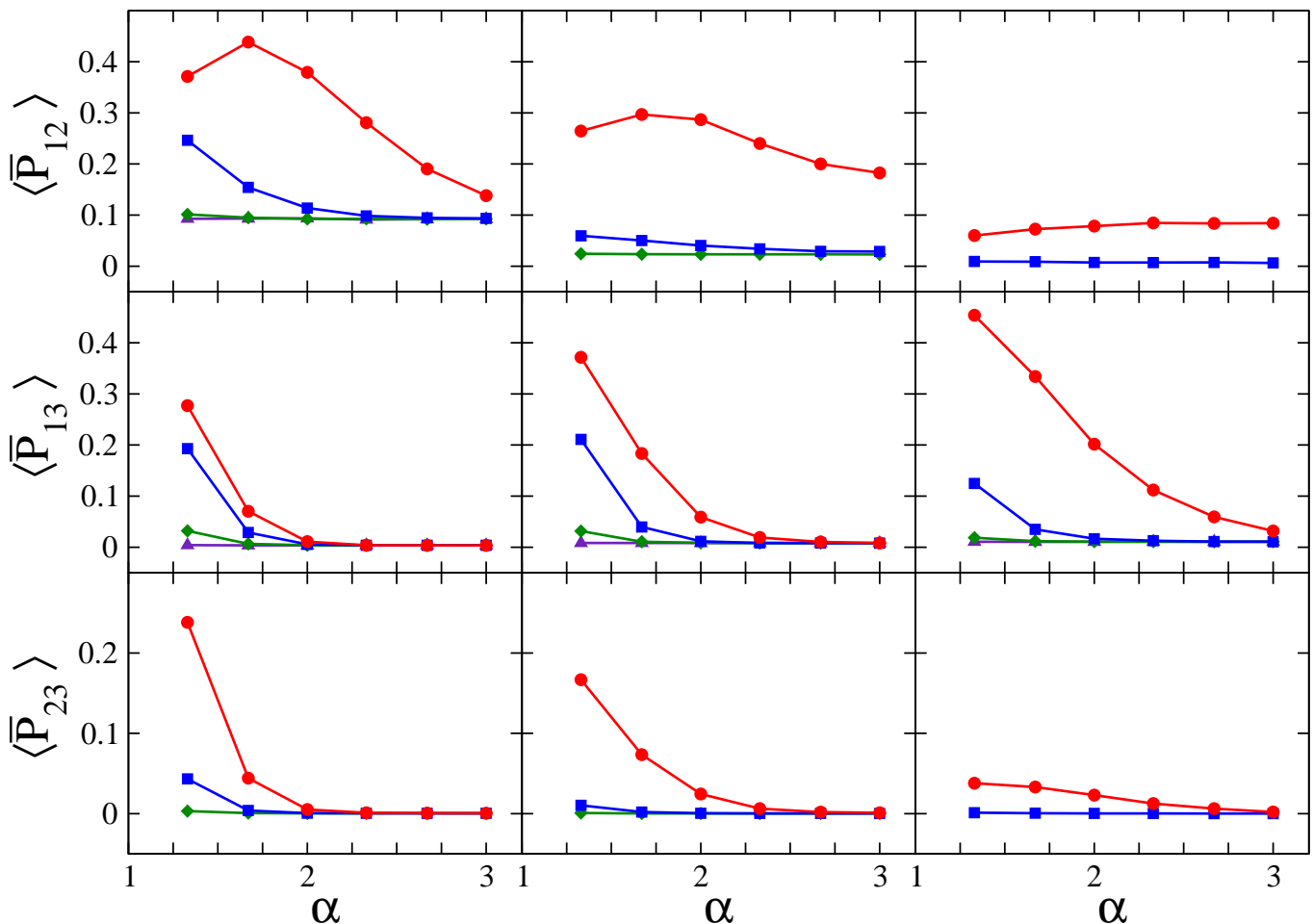


FIG. 14: The mean values of  $\bar{P}_{12}$  (top row),  $\bar{P}_{13}$  (middle row) and  $\bar{P}_{23}$  (bottom row) as a function of the power spectral index. The leftmost column is for 5 MeV neutrinos, the middle for 15 MeV and the rightmost is 45 MeV. In all panels the curves correspond to  $C_\star = 0.5$  (filled circles),  $C_\star = 0.3$  (filled squares),  $C_\star = 0.1$  (filled diamonds),  $C_\star = 10^{-2}$  (filled triangles). For the sake of clarity, not all lines appear in each panel.

the antineutrinos. In figures (14) and (15) we show the results for the means and standard deviations of the ensembles of antineutrino transition probabilities. A quick glance back at figures (4) and (5) shows that  $\bar{P}_{13}$  and  $\bar{P}_{23}$  are quite different from  $P_{13}$  and  $P_{23}$ . The antineutrino channel which is most sensitive to the turbulence is  $\bar{P}_{12}$  and this sensitivity is similar to the sensitivity of  $P_{12}$ . We also observe that at the largest value of  $C_\star$  shown, the evolution of  $\langle \bar{P}_{13} \rangle$  and  $\bar{\sigma}_{13}$  with the antineutrino energy appears to be counter that of  $\langle \bar{P}_{12} \rangle$ ,  $\langle \bar{P}_{23} \rangle$ ,  $\bar{\sigma}_{12}$  and  $\bar{\sigma}_{23}$ . Comparing figures (16) and (2) shows that the changes in  $P_{12}$  and  $\bar{P}_{12}$  are occurring when the density is between the H and L resonances for the  $E = 5$  MeV and  $E = 15$  MeV neutrinos. In this region the eigenvalue splitting  $\delta k_{12}$  and  $\delta \bar{k}_{12}$  are both approximately equal to the MSW potential  $V_{ee}$  and so the coupling between the states,  $U_{ei} U_{ej}^*$  and  $\bar{U}_{ei} \bar{U}_{ej}^*$ , are also approximately equal. This equivalence means it is as easy to stimulate a transition between states  $\bar{\nu}_1$  and  $\bar{\nu}_2$  as it is between  $\nu_1$  and  $\nu_2$  so the response to the turbulence will be the same.

Apart from  $\bar{P}_{12}$  at  $E = 5$  MeV, in order to explain these results we must use the stimulated transition model. A description of the turbulence effects upon the antineutrinos for a normal hierarchy in terms of induced MSW resonances would obviously not work well because there are no resonances in the antineutrino mixing channels. As we shall show, the distorted phase model only operates for  $\bar{P}_{12}$  at  $E = 5$  MeV; in all other channels and energies it does not operate because the adiabaticity of the transitions for the antineutrinos across the discontinuities in the profile are large. Further evidence that the stimulated model must be invoked is shown in figure (16) which shows the evolution of  $\bar{P}_{12}$ ,  $\bar{P}_{13}$ , and  $\bar{P}_{23}$  as a function of  $r$  for the exact same realization of turbulence used for figure (8). Note again the changes in  $\bar{P}_{12}$  occur before the jumps in  $\bar{P}_{13}$ . One can find a very similar figure in Patton, Kneller & McLaughlin [53] where it was demonstrated that the stimulated transition model correctly predicts the locations of the changes in probability. The absence of distorted phase effects in the majority of

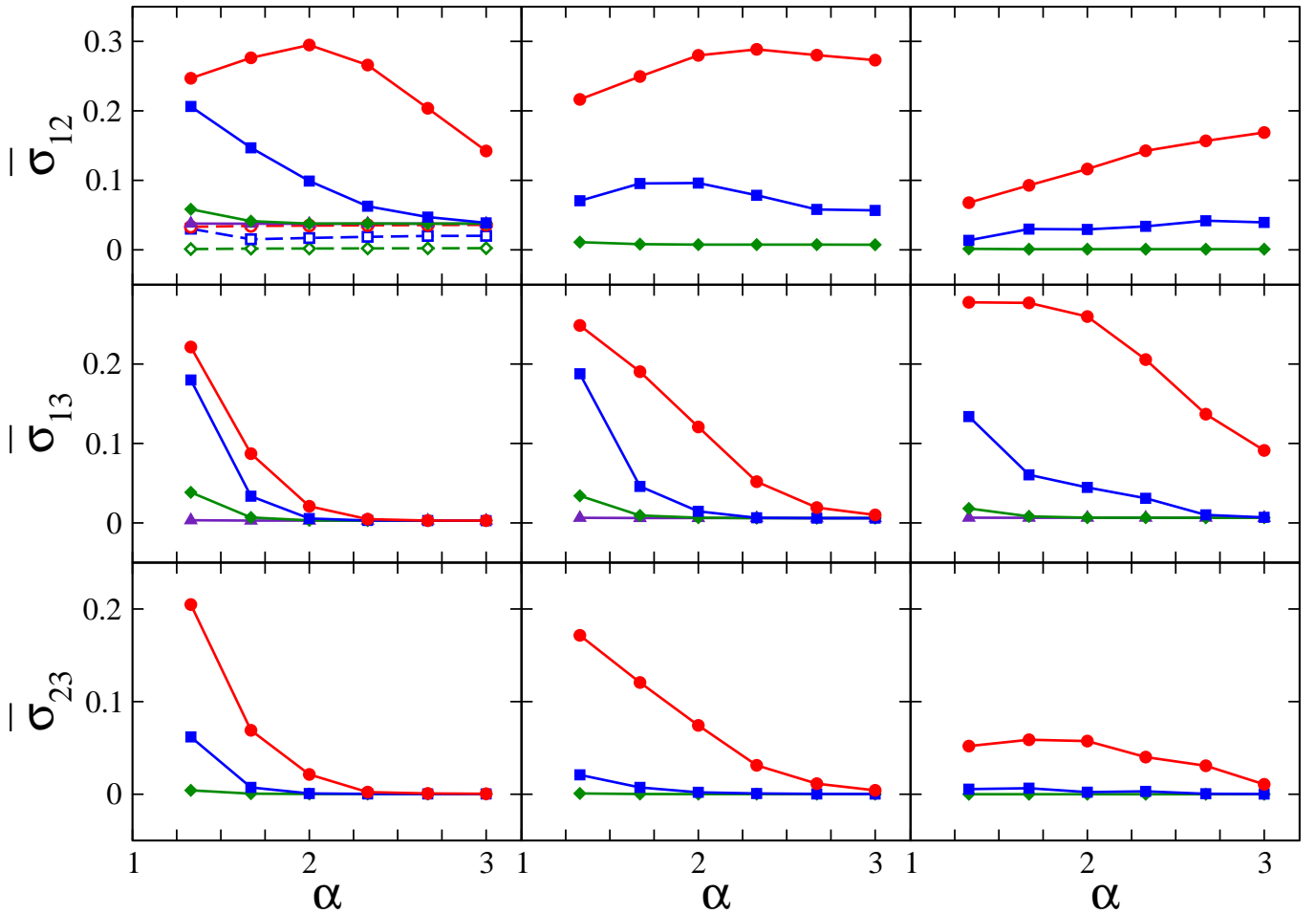


FIG. 15: The standard deviation of  $\bar{P}_{12}$  (top row),  $\bar{P}_{13}$  (middle row) and  $\bar{P}_{23}$  (bottom row) as a function of the power spectral index. The leftmost column is for 5 MeV neutrinos, the middle for 15 MeV and the rightmost is 45 MeV. In all panels the curves correspond to  $C_* = 0.5$  (filled circles),  $C_* = 0.3$  (filled squares),  $C_* = 0.1$  (filled diamonds),  $C_* = 10^{-2}$  (filled triangles),  $C_* = 10^{-3}$  (open circles),  $C_* = 10^{-4}$  (open squares) and  $C_* = 10^{-5}$  (open diamonds). Again, for the sake of clarity, not all lines appear in each panel.

the results shown in figures (14) and (15) makes their interpretation much easier than the neutrino transition probabilities.

That the antineutrinos are less sensitive to the turbulence amplitude is explained by the difficulty of stimulating transitions between antineutrino states as compared to the neutrino states in the normal hierarchy is. The difficulty is twofold: first the splitting between the eigenvalues are larger which means we require shorter wavelength Fourier modes in order to fulfill the parametric resonance condition and, with an inverse power law power spectrum, the amplitudes of these modes are smaller. Secondly the coupling between the states,  $U_{ei}U_{ej}^*$ , is also generally smaller in the antineutrinos. Both smaller amplitudes for the resonance modes and smaller coupling lengthen the distance over which the transition occurs making any transitions smaller. It requires very large  $C_*$  before stimulated transitions cause a noticeable effect in the antineutrino mixing channels as figures (14) and (15)

indicate. Hardening the spectrum has the simultaneous effect of raising the amplitude of the resonance modes and decreasing the amplitudes of modes which cause suppression so we expect a strong dependence upon  $\alpha$  up to the point where the combination of large amplitude and hardness of the turbulence power spectrum means the antineutrinos reach depolarization. Beyond that point, the dependence upon amplitudes and power spectral indices is lost. From figures (14) and (15) it appears a two-flavor depolarization is approached in  $\bar{P}_{12}$  for  $E = 5$  MeV and  $\alpha \lesssim 2$  and in  $\bar{P}_{13}$  for  $E = 45$  MeV and  $\alpha \sim 4/3$  only when  $C_* = 0.5$ .

Except in these few cases, inspection reveals the distributions of the probabilities are, again, mixtures. The distributions for  $\bar{P}_{12}$  when  $E = 45$  MeV and  $C_* = 0.5$  are mixtures of sharp, zero-peaked distribution and an exponential distribution. The fraction  $\bar{f}_{exp}$  of antineutrinos exponentially distributed for  $E = 45$  MeV and  $C_* = 0.5$  are shown in figure (7). We observe  $\bar{f}_{exp} = 25\%$

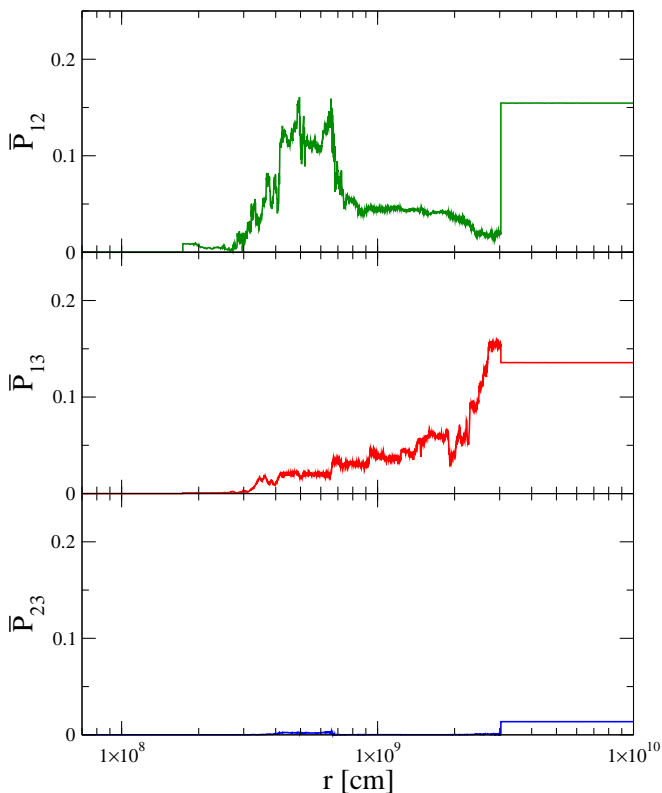


FIG. 16: The evolution of  $\bar{P}_{12}$  (top panel),  $\bar{P}_{13}$  (middle panel), and  $\bar{P}_{23}$  (bottom panel) as a function of distance  $r$  through the same realization of turbulence used for figure (8) i.e. with spectral index  $\alpha = 5/3$  and  $C_\star = 0.3\%$ . The antineutrino energy is 5 MeV.

at  $\alpha = 3$  and  $\bar{f}_{exp} = 78\%$  at  $\alpha = 4/3$  and again varies as  $\bar{f}_{exp} \propto 1/\alpha^{3/2}$ . These fractions are similar to those of the neutrinos. A difference does emerge when one examines the mean value of  $\bar{P}_{12}$  of the exponentially distributed subset. As with the neutrinos  $\langle \bar{P}_{12} \rangle_{exp}$  increases with  $\alpha$  but now we find that it grows linearly with the spectral index:  $\langle \bar{P}_{12} \rangle_{exp} = 7\%$  at  $\alpha = 4/3$  which has changed to  $\langle \bar{P}_{12} \rangle_{exp} = 33\%$  at  $\alpha = 3$ . This evolution is shown in the bottom panel of figure (7). The decrease of  $\bar{f}_{exp}$  and increase of  $\langle \bar{P}_{12} \rangle_{exp}$  as the power spectrum softens no longer cancel and we observe the counterintuitive increase of  $\langle \bar{P}_{12} \rangle$  and  $\bar{\sigma}_{12}$  with  $\alpha$ . A similar explanation can be used for the observed increase of  $\bar{\sigma}_{12}$  at  $C_\star = 0.3$  for this same energy of  $E = 45$  MeV.

Further evidence for larger stimulated transitions in a decreasing population is seen in figure (17) where we plot the frequency distributions of  $\bar{P}_{12}$  at the energy of  $E = 15$  MeV and  $C_\star = 0.3$ . The two mixing distributions are clearly seen in the bottom panel where  $\alpha = 2$  and we also see in the figure how large values of  $\bar{P}_{12}$  become populated as the spectrum softens. At  $\alpha = 4/3$  the mixing distributions are a sharp, zero-peaked distribution and an exponential; at  $\alpha = 2$  this has changed to a sharp, zero-peaked distribution and a two-flavor depolarized distribution. These distributions can be compared

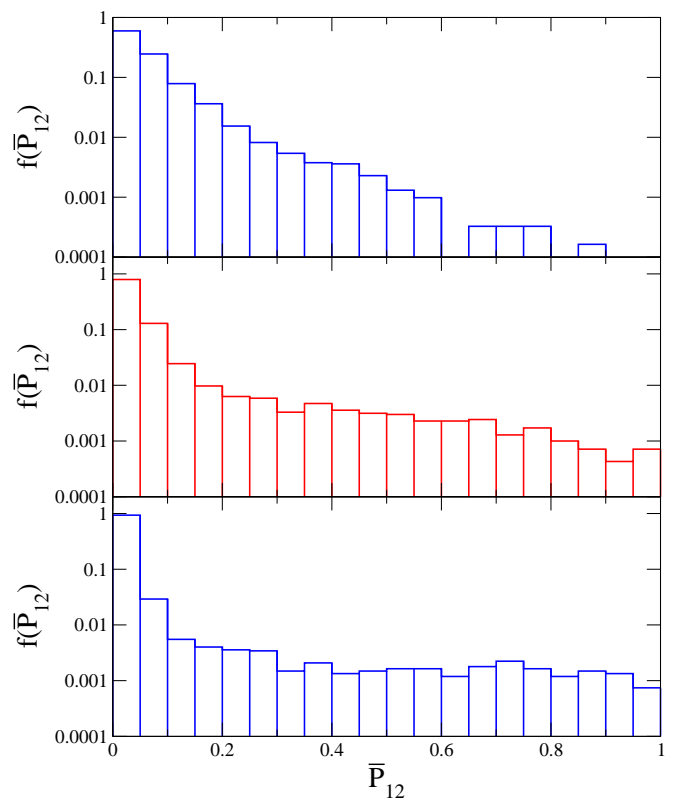


FIG. 17: The frequency distribution of the antineutrino transition probability  $\bar{P}_{12}$  when  $E = 15$  MeV and  $C_\star = 0.3$ . In the top panel  $\alpha = 4/3$ , in the middle  $\alpha = 5/3$ , and in the bottom panel  $\alpha = 2$ .

with those of  $P_{12}$  in figure (13) for the same energy.

Finally, the mixing channel  $\bar{P}_{13}$  is also, generally, a mixture of exponential and narrow distribution which peaks at zero. The two cases shown which do not match this pattern are for the  $E = 15$  MeV and  $E = 45$  MeV antineutrinos at  $C_\star = 0.5$  and  $\alpha \lesssim 5/3$  where the distribution is very close uniform. As with other cases the fraction of exponentially distributed transition probabilities  $\bar{P}_{13}$  strongly depends upon both  $C_\star$  and  $\alpha$  and is shown for all three energies in figure (18). The apparent inverse relationship between the sensitivity of  $\bar{P}_{13}$  to turbulence and the antineutrino energy is due to the larger coupling for the  $E = 45$  MeV antineutrinos compared to  $E = 5$  MeV. The antineutrino H resonance densities are negative and further from the densities seen in figure (1) for the  $E = 5$  MeV antineutrinos than for the for  $E = 45$  MeV.

## V. SUMMARY AND CONCLUSIONS

We have investigated the effect of modifying the turbulence power spectrum inserted into a supernova density profile upon the neutrinos and antineutrinos. The turbulence alters the transitions probabilities via two effects: the direct stimulation of transitions between the states

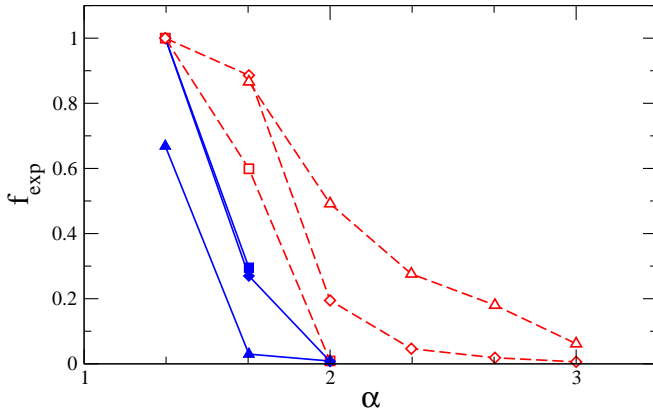


FIG. 18: The fraction of transition probabilities  $\bar{P}_{13}$  distributed according to an exponential. Solid symbols connected by solid lines are for  $C_\star = 0.3$ ; open symbols connected by dashed lines are for  $C_\star = 0.5$ . Squares for  $E = 5$  MeV, diamonds are  $E = 15$  MeV and triangles are  $E = 45$  MeV.

via parametric resonances, and the more subtle effect of changing the phase between semi-adiabatic resonances and/or discontinuities. The latter effect is only significant when the shocks and discontinuities in the profile are in the vicinity of the neutrino resonance densities - both L and H - and the mixing between antineutrino states  $\bar{\nu}_1$  and  $\bar{\nu}_2$  at low energy. The direct effect can operate in all mixing channels but, again, is strongest in the H and L resonant channels and between antineutrino states  $\bar{\nu}_1$  and  $\bar{\nu}_2$ . The two effects depend upon the turbulence power spectrum in different fashions complicated by the strong dependence upon the turbulence amplitude and other factors such as the progenitor structure, the post-bounce epoch, and the neutrino energy.

For a normal hierarchy and small amplitudes,  $C_\star \lesssim 1\%$ , turbulence impacts only the mixing between  $\nu_2$  and  $\nu_3$  significantly at the epoch of  $t \sim 3$  s postbounce for typical supernova neutrino energies of 5 MeV to 45 MeV. An effect from turbulence appears in the mixing between states  $\nu_1-\nu_2$  and  $\bar{\nu}_1-\bar{\nu}_2$  only at low energies at this same snapshot time: as the explosion progresses the higher energies will eventually show similar effects. In this region of parameter space the effect of turbulence enters through the distorted phase effect channel and we emphasize that even though the amplitudes are small, the effect upon the transition probabilities is significant. The distorted phase effect of turbulence does not disappear until  $C_\star \lesssim 10^{-4}$ . The distorted phase effect has a strong and weak limit: in the strong limit the phase between discontinuities is distributed uniformly leading to arcsine distributions for the transition probabilities. The parameters describing the arcsine distribution are determined by the jumps in the transition probabilities at the discontinuities not the turbulence between them. For this reason the mean and variance of the transition probabilities are not affected

by changes in the power spectrum. In the weak limit of the distorted phase effect the sensitivity to the power spectrum re-emerges due to the dominance of the long wavelength modes. Counterintuitively, this sensitivity to the longest wavelengths means harder spectra have *less* of an effect than soft spectra for a given  $C_\star$ .

The stimulated transition effect of turbulence emerges when the turbulence amplitude exceeds  $C_\star \gtrsim 1\%$  and appears in every mixing channel. Again, for a normal hierarchy at the epoch of  $t \sim 3$  s the channel most affected is the mixing  $\nu_2 - \nu_3$  with equivalent sensitivity for all three energies. The mixing between  $\nu_1-\nu_2$  and  $\bar{\nu}_1-\bar{\nu}_2$  are the next most sensitive to the turbulence with lower energies affected to a greater degree than higher at this epoch. This is understood as being due to the greater coupling between the states  $\nu_1$  and  $\nu_2$ . Stimulated transition also possess a strong and weak limit. In the strong limit the distributions of the transition probabilities are depolarized, either two or three flavor, while in the weak limit the distributions are found to be exponential. Although the two and three flavor depolarized distributions themselves do not depend upon  $\alpha$ , the boundary between them and distributions with exponential distributions does depend upon the power spectral index and the turbulence amplitude  $C_\star$  with a greater proportion of depolarization when the power spectrum is hardened at fixed  $C_\star$ . When depolarization is not significant the distributions of the transition probabilities in all channels are mixtures of more elemental distributions with the fraction of neutrinos that experienced stimulated transitions decreasing with the turbulence amplitude and softer power spectra.

Thus it appears there is little sensitivity to the power spectral index at the extremely large amplitude extreme when depolarization occurs and at small  $C_\star$  when the strong distorted phase effects dominate. In between, there is window of turbulence amplitudes in the range  $1\% \lesssim C_\star \lesssim 30\%$  where the spectral power index  $\alpha$  could play a role in shaping the transition probabilities. This is a very reasonable range of turbulence amplitudes to expect to find in hydrodynamical simulations and indicates further analyses along the lines of Borilleo *et al.* [26] are needed - particularly for 3D simulations. In future work we plan is to study the sensitivity of the correlation of the transition probabilities between neutrinos emitted along parallel rays from a finite size source.

### Acknowledgments

This work was supported by DOE grant DE-SC0006417, the Topical Collaboration in Nuclear Science “Neutrinos and Nucleosynthesis in Hot and Dense Matter”, DOE grant number DE-SC0004786, and an Undergraduate Research Grant from NC State University.

- 
- [1] Milisavljevic, D., & Fesen, R. A. *Astrophys. J.* **772** 134 (2013)
- [2] Mazzali, P. A., Kawabata, K. S., Maeda, K., et al. *Science* **308** 1284 (2005)
- [3] Tanaka, M., Kawabata, K. S., Hattori, T., et al. *Astrophys. J.* **754** 63 (2012)
- [4] Murphy, J. W., & Meakin, C., *Astrophys. J.* **742** 74 (2011)
- [5] Dolence, J. C., Burrows, A., Murphy, J. W., & Nordhaus, J., arXiv:1210.5241 (2012)
- [6] Ott, C. D., Abdikamalov, E., Moesta, P., et al., arXiv:1210.6674 (2012)
- [7] Hanke, F., Marek, A., Müller, B., & Janka, H.-T., *Astrophys. J.* **755** 138 (2012)
- [8] Pejcha, O., & Thompson, T. A., *Astrophys. J.* **746** 106 (2012)
- [9] Müller, B., Janka, H.-T., & Heger, A., *Astrophys. J.* **761** 72 (2012)
- [10] Takiwaki, T., Kotake, K., & Suwa, Y., *Astrophys. J.* **749** 98 (2012)
- [11] Lentz, E. J., Bruenn, S. W., Harris, J. A., et al., arXiv:1301.1326 (2013)
- [12] Tamborra, I., Hanke, F., Janka, H.-T., et al., *Astrophys. J.* **792** 96 (2014)
- [13] Abdikamalov, E., Ott, C. D., Radice, D., et al. arXiv:1409.7078 (2014)
- [14] Couch, S. M., & O'Connor, E. P. 2014, *Astrophys. J.* , 785, 123
- [15] Loreti, F. N. and Qian, Y.-Z. and Fuller, G. M. and Balantekin, A. B., *Phys. Rev. D* **52** 6664 (1995)
- [16] G. Fogli, E. Lisi, A. Mirizzi and D. Montanino, *JCAP* **0606** 012 (2006) [arXiv:hep-ph/0603033]
- [17] A. Friedland and A. Gruzinov, arXiv:astro-ph/0607244
- [18] S. Choubey, N. P. Harries and G. .G. Ross, *Phys. Rev. D* **76** 073013 (2007)
- [19] Kneller, J. and Volpe, C., *Phys. Rev. D* **82** 123004 (2010)
- [20] G. Reid, J. Adams and S. Seunarine, *Phys. Rev. D* **84** 085023 (2011)
- [21] J. P. Kneller, G. C. McLaughlin and K. M. Patton, *J. Phys. G* **40** 055002 (2013)
- [22] T. Lund, and J. P. Kneller, *Phys. Rev. D* **88** 023008 (2013)
- [23] Patton, K. M., Kneller, J. P., & McLaughlin, G. C., *Phys. Rev. D* **89** 073022 (2014)
- [24] Kneller, J. P., & McLaughlin, G. C., *Phys. Rev. D* **73** 056003 (2006)
- [25] Dasgupta, B., & Dighe, A., *Phys. Rev. D* **75** 093002 (2007)
- [26] Borriello, E., Chakraborty, S., Janka, H.-T., Lisi, E., & Mirizzi, A. arXiv:1310.7488 (2013)
- [27] Kifonidis, K., Plewa, T., Scheck, L., Janka, H.-T., Müller, E. *A&A* **453** 661 (2006)
- [28] Gkioulekas, E., & Tung, K.-K. *Journal of Low Temperature Physics* **145** 25 (2006)
- [29] Nastrom, G. D., & Gage, K. S. *Journal of Atmospheric Sciences* **42** 950 (1985)
- [30] S. P. Mikheev and A. I. Smirnov, *Nuovo Cimento C* **9** 17 (1986)
- [31] L. Wolfenstein, *Phys. Rev. D* **17** 2369 (1978)
- [32] Duan, H., Fuller, G. M., & Qian, Y.-Z. *Annual Review of Nuclear and Particle Science*, 60, 569 (2010)
- [33] Z. Maki M. Nakagawa and S. Sakata, *Prog. Theor. Phys.*, **28** 870 (1962)
- [34] J. Beringer et al. (Particle Data Group), *Phys. Rev. D* **86** 010001 (2012)
- [35] P. Langacker, S. T. Petcov, G. Steigman, and S. Toshev, *Nuclear Physics B*, **282**, 589 (1987)
- [36] Kneller, J. P., & McLaughlin, G. C., *Phys. Rev. D* **80** 053002 (2009)
- [37] Galais, S., Kneller, J., & Volpe, C., *Journal of Physics G Nuclear Physics*, **39** 035201 (2012)
- [38] Botella, F. J., Lim, C.-S., & Marciano, W. J. 1987, *Phys. Rev. D* , 35, 896
- [39] Esteban-Pretel, A., Pastor, S., Tomàs, R., Raffelt, G. G., & Sigl, G. *Phys. Rev. D* **77**, 065024 (2008)
- [40] Gava, J., & Jean-Louis, C.-C. *Phys. Rev. D* , 81, 013003 (2010)
- [41] Kramer, P. R., Kurbanmuradov, O., & Sabelfeld, K. *Journal of Computational Physics* **226** 897 (2007)
- [42] Kneller, J. P., & Mauney, A. W. *Phys. Rev. D* **88** 025004 (2013)
- [43] J. P. Kneller and A. W. Mauney, *Phys. Rev. D* , **88**, 045020 (2013)
- [44] T. Fischer, S. C. Whitehouse, A. Mezzacappa, F.-K. Thielemann and M. Liebendörfer, *A&A* **517A** 80F (2010)
- [45] Arcones, A., Janka, H.-T., & Scheck, L. *A&A* **467**, 1227 (2007)
- [46] Kneller, J. P., McLaughlin, G. C., & Brockman, J. *Phys. Rev. D* **77**, 045023 (2008)
- [47] V. K. Ermilova, V. A. Tsarev and V. A. Chechin, *Kr. Soob. Fiz. Lebedev Institute*, **5**, 26 (1986)
- [48] E. K. Akhmedov, *Sov. J. of Nuclear Physics*, **47**, 301, *Yad. Fiz.*, **47**, 475 (1988)
- [49] P. I. Krastev and A. Y. Smirnov, *Phys. Lett. B*, **226**, 341 (1989)
- [50] A. B. Balantekin, J. M. Fetter and F. N. Loreti, *Phys. Rev. D*, **54**, 3941 (1996)
- [51] M. Koike, T. Ota, M. Saito and J. Sato, *Phys. Lett. B*, **675**, 69 (2009)
- [52] Dyson, F. J., *Journal of Mathematical Physics* **3** 140 (1962)
- [53] Patton, K. M., Kneller, J. P., & McLaughlin, G. C. 2014, arXiv:1407.7835